PCCP

Accepted Manuscript

ROYAL SOCIETY OF CHEMISTRY

www.rsc.org/pccp

Unusual bonding modes of perfluorobenzene in its polymeric (dimeric, trimeric and tetrameric) forms: Entirely negative fluorine interacting cooperatively with entirely negative fluorine

Pradeep R. Varadwaj,[1] Arpita Varadwaj, Bih-Yaw Jin[1]

Department of Chemistry, National Taiwan University, Section 4, Roosevelt Rd, Taipei, 10617, Taiwan (R.O.C.)

Abstract

The $F^{\delta-}\cdots F^{\delta-}$ intermolecular synthon was recently observed useful for generating a two-dimensional layered supramolecular architecture on the Ag(111) surface (*Kawai et al., ACS Nano, 2015*). This was formed when the entirely negative covalently bound fluorine atoms in phenyleneethynylene(bis(2,3,5,6-tetrafluoro-4-(2,3,4,5,6-pentafluorophenylethynyl)phenyl)-ethyne (BPEPE-F18) were in close proximity to the same atoms in another BPEPE-F18 molecule. With a view to provide rigorous insights into the physical chemistry of such an intermolecular synthon, we have selected perfluorobenzene (C_6F_6) as a model compound, and have performed extensive DFT-M06-2X/6-311++G(d,p) investigations on a number of its homomolecular dimers, trimers, and tetramers. Of the twelve $(C_6F_6)_2$ dimers investigated, a displaced-parallel arrangement with an uncorrected binding energy (ΔE) of –7.4 kcal mol^{-1} was found to be the most stable, and an incorporation of the basis set superposition error (BSSE) has significantly reduced its ΔE to –4.7 kcal mol^{-1}. Besides, the ΔE for a minimum-energy least stable conformation of the same dimer, which involves a single $\sigma_{hole}(-)\cdots\sigma_{hole}(-)$ type $F^{\delta-}\cdots F^{\delta-}$ intermolecular bonding interaction, amounts to –0.62 and –0.24 kcal mol^{-1} without and with BSSE. The geometry of another conformation of the dimer, which accompanies a set of three $F^{\delta-}\cdots F^{\delta-}$ intermolecular interactions somehow similarly with those observed in the supramolecular layer formed of the BPEPE-F18 molecules, lies at a relative energy of 6.5 kcal mol^{-1} above the most stable conformation. Passing from this latter dimer to an analogous $(C_6F_6)_3$ trimer, as well as that from the trimer to an analogous $(C_6F_6)_4$ tetramer, each of the latter two clusters comprising of windmill-type $F^{\delta-}\cdots F^{\delta-}$ intermolecular topologies, we have marked a preferential increase in the value of ΔE from –0.94 (dimer) to –2.76 (trimer) to –4.49 kcal mol^{-1} (tetramer), thereby suggesting the presence of cooperative binding. An energy decomposed analysis has revealed that dispersion and polarization are the principal driving forces bringing the C_6F_6 molecules together in complex configurations. While a reasonable agreement was found between the charge density based topological results of the intermolecular bonding interactions emerged from applications of Quantum Theory of Atoms in Molecules (QTAIM) and Reduced Density Gradient approaches to all the polymeric compounds, the results of the latter method were found to be too vague especially near at the ring critical point regions. QTAIM's source function analysis has suggested that the fully negatively charged fluorine atoms in C_6F_6 serve as sinks for the $F^{\delta-}\cdots F^{\delta-}$ bond formations.

1. Introduction

Halogen bonding analogous in many senses to hydrogen bonding is a biologically and crystallographically dominant noncovalent interaction.[1] Owning to its ginormous applicability in the design of novel functional materials,[1-2] several research groups across the globe have joined together to form a Task Group in the past, which was then prompted to put forward rules governing its occurrence in compounds.[3] Although a number of characteristic properties have IUPAC recommended,[3] many of them have frequently been reflected in versatile bi- and multi-nary complexes involving medium-strong interactions of the covalently bound halogens. However, there are only a few of them that have

[1] Corresponding Author's Email Addresses: pradeep@t.okayama-uc.jp (PRV), byjin@ntu.edu.tw (BYJ)
Tel: +886-2-33661165, Fax: +886-2-23636359

been underrepresented. In particular, 'less than the sum of the van der Waals (vdW) radii (also called hard-sphere radii)' has recommended for its use as a geometric criterion in the search for halogen bonding and other σ_{hole} interactions, even though a use of this criterion was suggested some years ago to be a pitfall in the search for noncovalent interactions of the other type, such as hydrogen bonding.[4] The criterion often fails in border line cases wherein the covalently bound halogens involve with the negative sites in forming nocovalent interactions (i.e., for extremely weak interactions),[5] especially where the interplay between the higher order molecular momenta and/or dispersion portrays a major role in determining the interaction strength. There are two possible reasons that might explain this failure. Firstly, the vDW radii known for the atoms of the periodic table are not very accurate because they have been empirically determined based on the data measured using the varied nature of the measurement techniques and of the molecule type. Secondly, the covalently bound halogens in R–X (X = halogen, and R = remainder part of the molecule) do not occupy spherical volumes in space but are ellipsoidal due to the anisotropic distribution of charge density around the halogen nucleus, meaning that the radius of X along the extended R–X bond axis is smaller than that perpendicular to this axis, [6] and the effective vDW radii that have been evaluated and reported using the two types of radii mentioned just above might be erroneous. It must also be kept in mind that the magnitude of the vDW radius of an atom in its free state might always be different from that when it is covalently bound to other atoms in molecules, as well as when it is noncovalently bound to other atoms/bonds in other molecules (that is to say, the magnitude the vDW radius of an atom varies with the varying nature of the chemical environment). Although these issues are not the central concerns rather the main focus of the paper is to greatly enhance our current understanding of the efficiency of the covalent bound fluorine atom in molecules in forming noncovalent interactions with the negative sites.

Fluorine is the largest electronegative element among the four members of the halogen family. It is one of the potential candidates in medicinal chemistry, roughly 20-30% of the currently marketed drugs contain at least one fluorine atom.[7] It is also the least polarizable element in the halogen family, and its polarizability compared to the other halogens follows this order: F < Cl < Br < I, an order that is oppositely to their electronegativities (i.e., F > Cl > Br > I). [8] Because of these conspicuous eccentricities, the stability of the X'···X–R type-II halogen bonds, Scheme 1, formed between the covalently bound halogens R–X and the negative sites X' generally follows the order: (F <) Cl < Br < I, an order which is true regardless of the varying nature of the electron donor atoms X' involved.[9]

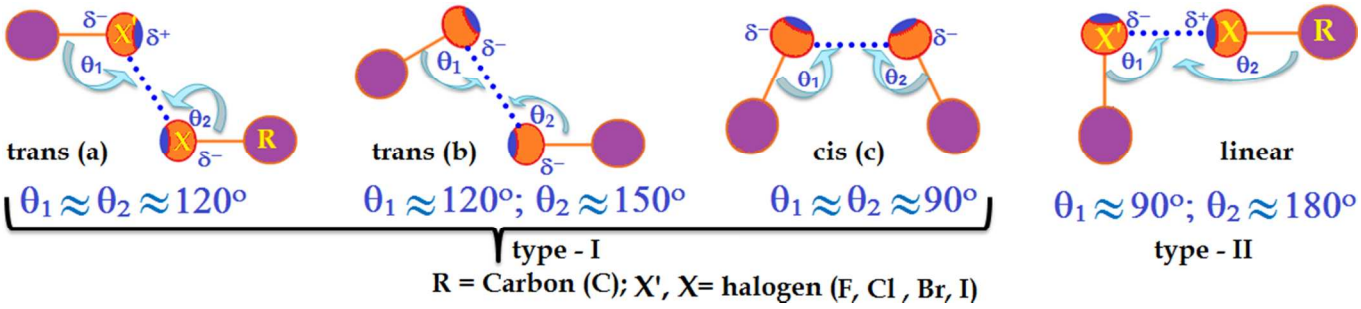

Scheme 1: Various modes of interaction of the covalently bound halogens

The covalently bound fluorine in many fluorinated compounds is fully negatively charged, e.g., H_3C–F, H_5C_6–F, H–F, H_2N–F, H_3CO–F, HO–F, and Cl–F, etc.[10a] Because of this, and because of its extremely low polarizability compared to the other three halogens it has been said that the fluorine is not proficient for forming halogen bond, [9a, b, d] and therefore not typically considered as X-bond donors, [8e] though there are scientific views on the opposite. [10, 12]

The fluorine atoms in perflurometh ane (CF_4) were suggested to be solely negative, [11a] and according to Politzer et al., [9a, b,d] they are incapable of forming noncovalent interactions with the negative sites on other molecules, e.g., NH_3. Contrariwise, we have recently showed that this suggestion about the fluorine's bonding temperament in CF_4 is not true.

This is obviously due to the fact that the fluorine in this species accompanies a minuscule region of positive electrostatic potential (called σ_{hole}) domiciled on its surface along the outer extension of the C–F covalent bond.[5c] Consequently, such positive regions on the fluorine atoms could adequately form halogen bonded clusters when placed in close proximity to appropriate nucleophiles, such as the oxygen, nitrogen, and fluorine atoms of OCH_2, NH_3, and FH, respectively. [5c] The latter results are concordant not only with the conclusions of Osuna and coworkers, [40] as well as of Cormanich et al., [33e] both drawn theoretically, but also with the experimental results of Bol'shutkin et al. reported forty years ago, [48a] all on the dimers of CF_4. To pinpoint precisely about the experiment, it was observed that the fluorine atoms in the CF_4 subunit in the CF_4 crystal attract the same atoms in the neighboring CF_4 subunits, leading to the formation of diverse varieties of F···F intermolecular bonding linkages (ref codes TFMETH, [48a] TFMETH02, [48b] and TFMETH03[48c] (see Fig. S1 of ESI)).[39]

A suggestion homologous to the above was also presented in the past for chloromethane (H_3C–Cl). [11a-c] For example, it was initially suggested that the chlorine in H_3C–Cl is entirely negative, thus cannot halogen bond.[11a] However, Riley et al.[11d] were able to report a detailed theoretical study on the possibility of the H_2CO···Cl–CH_3 gas phase dimer. Because the mechanism behind the formation of this dimer does not match with their earlier suggestion, the authors of ref.[11a] have further argued that the dimer must have formed due to the electric field of the oxygen atom in H_2CO which was sufficiently enough not only to polarize the chlorine atom in H_3C–Cl on their head on approaches, but also to induce a positive region on its electrostatic surface, which was then having the ability to interact attractively with the nucleophile associated with the oxygen atom in H_2CO.[11b-c] Contrarily, we have recently showed that this argument is perversely counterintuitive (see below further discussions), as the chlorine in H_3C–Cl has inherently have a positive σ_{hole} of its own on its outermost electrostatic surface, which was not induced by its partner species upon the electrostatic interaction, which could attract favorably the covalently bound nitrogen atoms of varied strengths of negative electrostatic potential in RN molecules.[5b]

Whereas the covalently bound fluorine in numerous fluorinated compounds is fully negative, there are a few reported exceptions, F_2, NCCCF, F_3CCF and FCN, for examples, for which, the charge density around the fluorine's nucleus is anisotropic.[10a,12] This generally leads to the lay understanding that in such compounds there must be an electron-deficient electrophilic cap of positive electrostatic potential (σ_{hole}) lying along the outermost extension of the covalently bound fluorine, and the lateral portions of it lying perpendicular to the σ-bond axis must be dominated with lone pairs of electrons, the latter is generally typified by a belt of negative electrostatic potential. The former and latter regions on atoms in molecules are generally visualized by the 0.001 a.u. charge density mapped molecular electrostatic surface potential graph. They are quantified by the signs and magnitudes of the local most surface maxima and minima of electrostatic potential, often represented by the symbols $V_{s,max}$ and $V_{s,min}$, respectively. [8,9,11] It was objectified that both $V_{s,max}$ and $V_{s,min}$ are useful measures of halogen bond strength.[5b,9,13]

The domiciliation of the electropositive cap on the outer surface of the fluorine in the R–F molecules (R–F = FCCF, NCF, NCCCF, F_3CCF and F_2) noted heretofore in this discussion, according to Politzer et al.,[12a-b] Li et al.,[12c] Lu et al.,[12d] and Eskandari et al.,[12e] was possible only because R was sufficiently electron-deactivating. Because of this cap, the fluorine in these molecules has showed its propitious potential to attract the Lewis base centers, e.g., as in NH_3, towards itself to form N···F weakly bonded interactions. They display many characteristics comparable with hydrogen bonding, as well with halogen bonding formed by the latter three heavier halogens (X = Cl, Br, and I). Eskandari and Lesani have recently argued that these interactions should be named as 'fluorine bond' rather than referring them to as 'halogen bond',[12e] although the term 'fluorine bond' has already been referred some time ago to represent similar other noncovalent interactions.[14] According to the authors, they have so-named the interaction because unlike the latter three halogens the covalently bound fluorine in each of the above five fluorinated compounds serves as a sink rather than as a source for the N···F interactions.

By contrast, the most recent experimental observations of Kawai et al. demonstrate that fully fluorinated aromatic compounds, viz. phenyleneethynylene(bis(2,3,5,6-tetrafluoro-4-(2,3,4,5,6-pentafluorophenylethynyl)phenyl)-ethyne (BPEPE-F18), can form C–$F^{\delta-}\cdots F^{\delta-}$–C intermolecular bonding interaction during supramolecular self-assembly.[15] To put it another way, the authors of that study have found the fluorine atoms in isolated BPEPE-F18 to be thoroughly negative, evidenced by the molecular electrostatic surface potential map (values not reported). They then have showed that these atoms of that species can promote to develop $F^{\delta-}\cdots F^{\delta-}$ attractive intermolecular interactions with the same atoms in another BPEPE-F18, leading to the formation of a two-dimensional supramolecular layered structure. This is an observation that advocates *like attracting like*, no matter, how electronegative are the σ_{holes} and the accompanying lateral sides of the fluorine atoms in BPEPE-F18. Although the serendipitous discovery, which encompasses the geometrical arrangement between the BPEPE-F18 monomers to be regulated in such a way as to form windmill type $F^{\delta-}\cdots F^{\delta-}$ intermolecular topologies, is very rare in the vast literature, it does not come along with the assertion of Politzer et al. [9e] *halogen bonding readily be understood as the attractive interaction between the positive outer region on the halogen and the negative site*. In any case, we would like to clarify that the anisotropic fluorine in BPEPE-F18 must have an entirely negative σ_{hole} on its outer electrostatic surface along the extension of the C–F bond, a view which is in contrast with Kawai et al.[15] who have exaggerated its absence. We believe that their interpretation was fully based on the fact that the negative σ_{hole} region on the fluorine surface could be indistinguishable on the electrostatic surface of the BPEPE-F18 molecule as it merges with its negative lateral regions.

Given the profound importance of $\pi\cdots\sigma$, lone-pair$\cdots\sigma$, and π—π interactions, etc., in many areas of chemistry, biology, and crystal engineering, we have attempted in this study to explore similar such bonding interactions in the dimers the perfluorobenzene (C_6F_6) molecule, and to a lesser extent, trimers, and tetramers. Our primary aim towards this study was (i) to examine whether the similarly charged fluorine atoms can form C–$F^{\delta-}\cdots F^{\delta-}$–C intermolecular bonding interactions in the conformations of the $(C_6F_6)_{n(n = 2, 3, 4)}$ clusters, and whether their bonding characteristics can be directly comparable with the ones observed experimentally in the layered supramolecular structure formed of the BPEPE-F18 molecules, [15] (ii) to verify its persuasiveness and impact in underpinning the future self-assembly, and (iii) to better understand its underlying physical chemistry in terms of the intermolecular geometries, energetics, and topological features of the charge density. A particular interest was also placed to elucidate whether the $F^{\delta-}\cdots F^{\delta-}$ metric can be treated an effective tool to enhance the stability of a complex configuration. We have tackled this problem by examining the various $(C_6F_6)_{n(n = 2, 3, 4)}$ clusters involving the $F^{\delta-}\cdots F^{\delta-}$ intermolecular interactions. In doing so, we could comment on whether the self-assembled two-dimensional supramolecular structure formed of the BPEPE-F18 molecules on the Ag(111) surface[15] was the eventual repercussion of any cooperative phenomena.

In order to address the specific questions delineated above, we have employed Density Functional Theory (DFT) at the M06-2X/6-311++G(d,p) level of theory to calculate the equilibrium geometries and Hessian energy eigenvalues of the twelve conformations of the $(C_6F_6)_2$ cluster, of the three conformations of the $(C_6F_6)_3$ cluster, and of the two conformations of the $(C_6F_6)_4$ cluster. The efficacy of this methodology[16a,b] in handling noncovalent interactions has been the topic of various preceding studies,[9b,16c-f] thus is suitable for the current purpose. In addition, we have performed Molecular Electrostatic Surface Potential (MESP) analysis[17] at the same level of theory to determine the various minima and maxima of electrostatic potential on the surface of the C_6F_6 monomer, which, in turn, are generally required for enlightening the most important electrophilic and nucleophilic regions. Also, we have performed Quantum Theory of Atoms in Molecules (QTAIM) [18] and Reduced Density Gradient (RDG) [19] charge density based topological analyses to elucidate the nature of the closed-shell bonding interaction involved in every pair of two atomic basins in the equilibrium structures of the $(C_6F_6)_{n(n = 2, 3, 4)}$ clusters investigated. Computer codes such as Gaussian 09,[20a] Gamess, [20b] AIMALL, [21] MultiWfn, [17] and VMD [22] were utilized for electronic-structure and -density based calculations, visualizations, and graphics

generations. (Ultrafine integration grid and tight convergence criteria in lieu of default settings were invoked in the Hessian calculations performed with Gaussian 09.)

2. Results and discussion

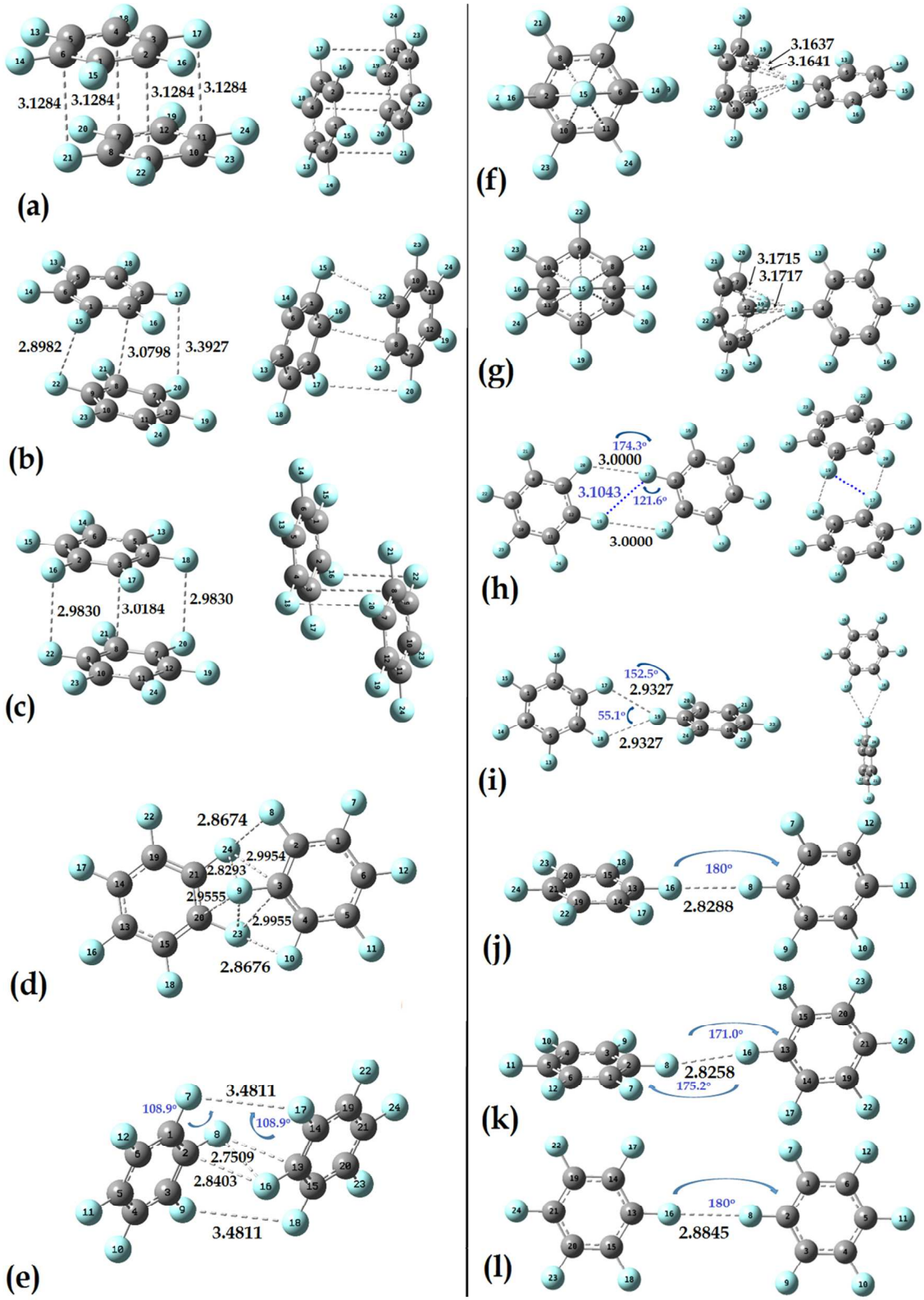

Fig. 1: The twelve optimized geometries of the $(C_6F_6)_2$ dimer, obtained using M06-2X/6-311++G(d,p). Bond-lengths (in Å) and -angles (in °) are given for some selected intermolecular contacts. For clarity, two different views are displayed for several geometries. The dotted lines between the atoms are drawn to show consistency with the QTAIM-based molecular graphs presented in Fig. 4, evocative of the presence of noncovalent interactions. Atom labeling is randomly shown. Due to symmetry, two nearly degenerate intermolecular bond distances are presented for geometries f) and g).

2.1 Structural and energetic landscapes of dimers

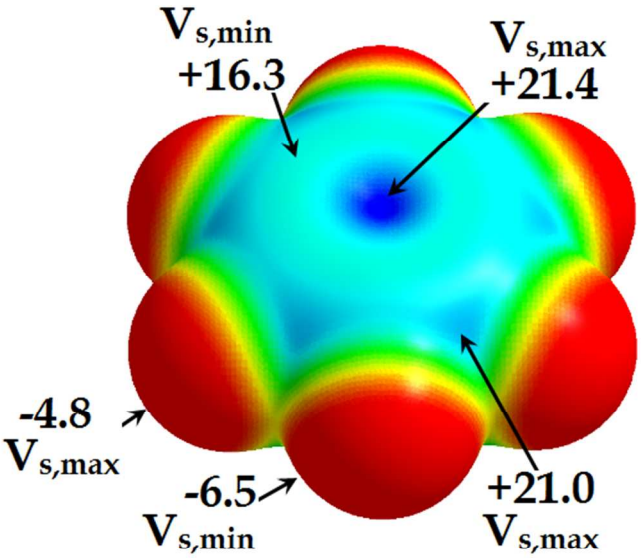

Fig. 2: M06-2X/6-311++G(d,p) computed molecular electrostatic surface potential of perfluorobenzene (C_6F_6), mapped with the 0.001 a.u. isodensity. Colors in red and deep blue represent the most negative and most positive regions of electrostatic potential, while those in yellow, green, and cyan represent the least negative, least positive, and more positive regions of electrostatic potential. $V_{s,min}$ and $V_{s,max}$ values are in units of kcal mol^{-1}. The deep-blue hole-like domain on the center of the ring surface is a π_{hole}.[9f,]

Fig. 1 illustrates the optimized geometries of the twelve conformations of the $(C_6F_6)_2$ dimer, and Table 1 lists their energetic properties. Of these, the most stable conformation is turn out to be the one with a favorable displaced-parallel arrangement, a. Its binding energy, ΔE, calculated using a supermolecular procedure we have previously employed,[5a-c, 23] is worth –7.38 kcal mol^{-1}. I is about 1.04 and 1.19 kcal mol^{-1} (see Δ values in Table 1) more stable than the configurations b and c (distorted and undistorted displaced-parallel), respectively. It is worth emphasizing that we had initially attempted at energy-minimizing two different sandwiched (on top parallel) geometries of the $(C_6F_6)_2$ dimer, despite the resulting conformations were turn out to be a and c. Why the on top parallel geometry of the $(C_6F_6)_2$ dimer was not found could probably be explained by the large nonbonded repulsion between the carbon faces associated with the six-membered rings of the two monomers on their head-on approaches. We believe this repulsion must have overpowered the corresponding attractive counterpart, thereby making the said geometry destabilized (unstable). This is not very dumbfound because the electrostatic potential at the outer surface the aromatic ring center in C_6F_6 is largely positive, $V_{s,max}$ = +21.4 kcal mol^{-1}, Fig. 2.

Compared to the previous suggestions for the $(C_6F_6)_2$ benzene dimer,[24] as well as that for similar other dimers,[25] it may be anticipated that each of the above three conformations (a-c) of the $(C_6F_6)_2$ dimer is $\pi\cdots\pi$ stabilized. This means quadrupolar and London dispersion interactions, the former supposedly yielding from the product of the polarizabilities the two π systems, are the key competitive contributing sources for the attraction between the two monomers. The incisive remark may be no wonder because C_6F_6 is a polar molecule that has a

Table 1: Selected energetic properties of the $(C_6F_6)_2$ dimers, obtained with M06-2X in conjunction with the 6-311++G(d,p) basis set. [a]

Conformation[a]	Relative stability (Δ)	ΔE	BSSE	ΔE (BSSE)
(a)	0.00	–7.38	2.67	–4.72
(b)	1.04	–6.35	2.20	–4.14
(c)	1.19	–6.20	2.23	–3.97
(d)	3.09	–4.30	1.35	–2.95
(e)	3.95	–3.44	1.26	–2.17
(f)	4.51	–2.88	1.16	–1.72
(g)	4.53	–2.87	1.16	–1.71
(h)	6.45	–0.94	0.51	–0.43
(i)	6.49	–0.90	0.49	–0.41
(j)	6.77	–0.62	0.38	–0.24
(k)	6.78	–0.61	0.46	–0.15
(l)	6.88	–0.51	0.33	–0.17

[a]The properties include the relative stability (Δ/kcal mol^{-1}), the binding energy (ΔE/kcal mol^{-1}), the basis set superposition error energy (BSSE/kcal mol^{-1}), and the BSSE corrected binding energy (ΔE(BSSE)/kcal mol^{-1}).
[b] See Fig. 1 for conformational details.

quadrupole moment (Θ) closely in magnitude but opposite in sign to C_6H_6, values of Θ –28.9±1.7 vs. +31.7±1.7 $Cm^2\times10^{-40}$ (experimental).[26] In an analogous slipped-parallel $(C_6H_6)_2$ dimer, it was argued that dispersion is the key driving force for complex stabilization, and electrostatics plays the role of repulsion.[50]

The geometries d and e (Fig. 1) are the other two high energy conformations of the $(C_6F_6)_2$ dimer. The former is a minimum and latter a second order saddle point (imaginary frequencies are –9.4 and –24.4 cm^{-1}, respectively). They are about 3.09 and 3.95 kcal mol^{-1} less stable than the conformer a. They both comprise of several short C···F and F···F contacts, the shortest and longest of these are ca. 2.7509 Å and 3.4811 Å, respectively. Similar to the conformations b and c, both d and e do involve type-Ic contact, Scheme 1. This could be realized by inspecting the values of 93.5 (93.5), 91.5 (91.5), 131.8 (82.9), and 108.9 (108.9°) obtained for the angles $\angle C_7$–F_{20}···F_{17} ($\angle F_{20}$···F_{17}–C_3), $\angle C_4$–F_{18}···F_{20} ($\angle F_{18}$···F_{20}–C_7), $\angle C_{21}$–F_{24}···F_8 ($\angle F_{24}$···F_8–C_2), and $\angle C_1$–F_7···F_{17} ($\angle F_7$···F_{17}–C_{14}) in b, c, d, and e, respectively.

The two C_{2v} geometries f and g (Fig. 1) of the $(C_6F_6)_2$ dimer are T-shaped (edge-face), both lying roughly at an elevated energy of 4.5 kcal mol^{-1} compared to the conformation a. These geometries, from the electrostatic surface potential point of view, are presumably stabilized by the $\pi_{hole}(+)\cdots\sigma_{hole}(-)$ interaction, the entirely positive π_{hole} in one C_6F_6 (the face of the ring) interacting with the fluorine's negative σ_{hole} in the other C_6F_6 (the edge), with the mean C···F intermolecular distances are ca. 3.1639 and 3.1716 Å for the corresponding dimers, respectively. Both the geometries are first order saddle points with the present level of theory, with the imaginary frequencies associated with the low-frequency deformation vibrational modes of the respective dimers are ca. –7.1 and –3.5 cm^{-1}, respectively. The topology is identical to what is commonly known as the T-shaped configuration of the $(C_6H_6)_2$ dimer that enjoys preferable quadrupole/quadrupole interactions, as it facilitates a favorable environment wherein the positive quadrupole of one C_6H_6 ring interacts attractively with the negative quadrupole of the other.

The geometries associated with the other two conformations h and i (Fig. 1) of the $(C_6F_6)_2$ dimer are both minima, with the former and latter belong to the C_{2h} and C_2 point group symmetries, respectively. The geometry of the former conformation is formed due to the quasilinear attraction between the fluorine's negative σ_{holes} in one monomer and the negative lateral portion of the same atoms in another monomer (lone-pair···$\sigma_{hole}(-)$ type). The two short F···F distances in this geometry are equivalent, 3.0000 Å each, both represented by the broken lines in white-gray. The angles θ_1 (θ_1 = $\angle C_7$–F_{20}···F_{17}) and θ_2 (θ_2 = $\angle F_{20}$···F_{17}–C_3) associated with these contacts are approximately 125.5 and 174.3°, respectively (see Scheme 1 for θ_1 and θ_2). Because the latter angle is close to 180°, one may conclude a strong directional preference of bonding in this dimer similarly with the type-II intermolecular topology (Scheme 1), which is generally formed when the covalently bound halogen with an electrophilic cap (of positive electrostatic surface potential) on it links with the nucleophilic sites through an attractive interaction. [27e-f]

In the geometry i, however, the fluorine's negative σ_{hole} in one monomer on the right is facing the mid-point of a C=C bond of another monomer on the left. The arrangement has resulted in an equivalent F···F pair formed between the lateral negative sides of the three interacting fluorine atoms. The intermolecular distance associated with the F···F equivalent pair is ca. 2.9327 Å, and the angles θ_1 and θ_2 associated with them each are approximately 122.4 and 152.5°, respectively. Interestingly, these values do not match with the previously defined type-I contacts, [27] we thus named it to be referred to as type-Ib, Scheme 1.

Noticeable in geometry h is another short F···F pair transpiring between the two C_6F_6 monomers. It is represented by the dotted line in blue, and is occurring between the lateral sides of the two fluorine atoms, each from a given monomer. Unlike the F···F pairs discussed already above, this latter is seemingly a forced interaction. The

intermolecular distance for this F···F pair is ca. 3.1043 Å, with $\theta_2 \approx \theta_1 = 121.6^o$. Interestingly enough, the angular feature associated with this interaction is analogous to what has been referred in the literature to as type-I contact,[6a, 27] but we called it type-Ia to discriminate it from type-Ib and –Ic contacts, Scheme 1. Such a topology of bonding is commonly

Table 2: Comparison of some selected physical properties of the D_{2d} geometry of the $(C_6F_6)_2$ dimer, obtained with various levels of theory in conjunction with the 6-311++G(d,p) basis set. [a,b]

Method[c]	r(F···F)	ΔE	ΔE (ZPV)	BSSE	(BSSE/ΔE)×100[e]	ΔE(BSSE)
MP2[d]	2.8306	–0.57	---	0.43	75.4	–0.14
M06-2X	2.8288	–0.62	–0.39	0.38	61.5	–0.24
ωB97XD	3.1666	–0.61	–0.47	0.34	56.5	–0.26
B3LYP-D	2.7825	–0.14	+0.04	0.35	260.4	+0.22
Cam-B3LYP	2.7949	–0.44	–0.30	0.34	77.8	–0.16
B3LYP	3.0603	–0.21	–0.10	0.29	136.3	+0.08
X3LYP	2.8813	–0.41	–0.28	0.33	80.8	–0.08
TPSSTPSS	3.0841	–0.39	–0.27	0.34	85.1	–0.06
PW91PW91	2.9182	–0.77	–0.64	0.36	46.4	–0.41
PBEPBE	2.9670	–0.47	–0.34	0.33	69.6	–0.14
PBE1PBE	2.9570	–0.44	–0.29	0.36	81.8	–0.08
HCTH	2.9701	–0.75	–0.61	0.31	41.9	–0.44
BHandHLYP	2.8286	–0.41	–0.25	0.35	86.2	–0.06

[a] See Fig. 1**j** for geometry.
[b] The properties include the F···F intermolecular bond distance (r/Å), the binding energy (ΔE/kcal mol^{-1}), the zero-point-vibration correction binding energy (ΔE(ZPV)/kcal mol^{-1}), the basis set superposition energy (BSSE/kcal mol^{-1}), the percentage $(BSSE/\Delta E)\times 100$ and the BSSE corrected binding energy (ΔE(BSSE)/kcal mol^{-1}).
[c] See ref. 45 for details about the DFT and DFT-D functionals investigated.
[d] MP2 calculation was performed in conjunction with the 6-311G(d,p) basis set. We were unable to perform the Hessian calculation at this level because our calculation has often encountered the g_write error.
[e] Percentages (%) are estimated considering the BSSE and ΔE values upto the three decimal places.

observed between the carbon bound halogen atoms in the solid state,[27] crystalline $(C_6Cl_6)_3$, for example.[27a] Recently, Duarte et al. have suggested a similar interaction topology between the bromine atoms in the FBr···BrF dimer, which was formed due to the interaction of a lump on one bromine with the hole on the other.[27b] According to Brammer et al.,[27c] this kind of geometrical attribute is a repercussion of an electrostatically repulsive arrangement since at the point of interaction their MESPs are nearly identical, and their occurrences are not very surprising in the solid state as they are most likely to result from minimization of intermolecular repulsions or from weakly attractive interaction driven by dispersive forces. Awwadi and coworkers have suggested that the C–X···X–C (X = Cl, Br, I) type-Ia interaction topology which is by far most common in the solid state is electrostatically attractive for a narrow range of angles, $140 < \theta_1 \approx \theta_2 < 160$, [27d] and beyond this range they are mostly electrostatically repulsive. However, as noted by Brammer et al., [27c] there exist some specific cases, wherein the C–X···X–C interactions beyond the above angular range are still attractive (similar to those found for the geometries h and i), and in those cases, dispersion plays an intervening role.

In each of the other three conformations of the $(C_6F_6)_2$ dimer, j-l, there is a single F···F intermolecular bonding interaction. The former one and latter two geometries of the dimers are stationary and first order saddle points, respectively (imaginary frequencies associated with the latter two are ca. –5.1 and –2.3 cm^{-1}, respectively). The F···F intermolecular distance is about 2.8288 Å in j (D_{2d}), 2.8258 Å in k (C_1), and 2.8845 Å in l (D_{2h}). The binding energies for the corresponding dimers are ca. –0.62, –0.61, and –0.51 kcal mol^{-1}, respectively, showing the F···F interaction strengths in these dimers are nearly equivalent. For the former and latter geometries, $\theta_1 \approx \theta_2 = 180^o$, revealing a prototype $\sigma_{hole}(-)\cdots\sigma_{hole}(-)$ interaction. For the intermediate geometry k, $\theta_1 = 171.0^o$ and $\theta_2 = 175.2^o$, and the F···F pair could also

be described as lone-pair$\cdots\sigma_{hole}(-)$ type. In most of these unconventional interactions, one of the fluorine atoms is probably serving as a fluorine bond acceptor, and the other as a fluorine bond donor.

The electrostatic fields around covalently bound fluorine atoms in isolated C_6F_6 are ostensibly equivalent. This may be realized from the negative electrostatic potential values that are computed to be identical on the surfaces of the fluorine atoms along (or around) the outer extensions of the C–F bond axes (cf. Fig. 2). Because of it, one must not expect an induction of a positive electrostatic potential on the surface of the fluorine atom in a monomer caused by the electrostatic fields of the same atoms in another monomer when both are on their head-on approaches. This proves the fact that for the formation of an F$\cdots$F link, as in the geometries h and l, one does not necessarily require an involvement of a positive site. The result is in sharp contrast with an assertion of Politzer et al. *the negative electrostatic potential associated with a σ_{hole} precludes the possibility of halogen bonding–unless the electric field of the negative site is strong enough to induce a positive region on the halogen*.[9a,b,d]

Nevertheless, it is well known that DFT is notoriously poor at accurately describing long-range effects, including dispersion. Although M06-2X can deliver some impressive accuracy for its expense but, like all parametrized models, is not necessarily guaranteed to perform well under all scenarios. For example, according to Zhao and Truhlar, the M06-2X outperforms many older DFT functionals, and offers reasonable chemical accuracies for applications in main-group thermochemistry, kinetics, and noncovalent interactions. [16a,b] Similarly, Kozuch and Martin have suggested only recently that the DFT functionals with high exact exchange or long-range corrections, especially M06-2X and ωB97XD, and double hybrids, are suitable for the study of halogen bonding, [16f] yet there are examples in the literature where this functional underperforms. [41] Taking this as an issue, we have reoptimized only the D_{2d} geometry of the $(C_6F_6)_2$ dimer j (Fig. 1) with eleven other very popular DFT and DFT-D functionals in conjunction with the same 6-311++G(d,p) basis set. The results listed in Table 2 manifest the F$\cdots$F distances to vary widely between 2.7949 (Cam-B3LYP) and 3.0841 Å (TPSSTPSS), and the uncorrected ΔE to vary between −0.14 (B3LYP-D) to −0.77 kcal mol^{-1} (PW91PW91). Indeed such a large variation in the intermolecular distances, as in the values of the ΔE, can be attributed to the percentage of exchange and correlation mixing in the DFT functionals. Among the functionals tested, the ΔE determined with M06-2X is harmonious with that obtained with ωB97XD, as well as with that calculated with the highest level of theory applied (MP2), thereby demonstrating trustworthiness of the M06-2X results. However, compared to M06-2X, all the other DFT/DFT-D functionals have underestimated the ΔE, except for PW91PW91, ωB97XD, and HCTH, in which cases, there were slight overestimations. In contrary, the B3LYP functional significantly underestimates the ΔE which is also not unacceptable because it does not properly incorporate long-range forces. [42]

Table 1 summarizes the basis set superposition error (BSSE) energies for all the $(C_6F_6)_2$ dimers examined, estimated using the counterpoise procedure of Boys and Bernardi[43a] with M06-2X. As can be readily seen from the data, the BSSE is as large as 2.67 kcal mol^{-1} for the most stable dimer a, and is as small as 0.33 kcal mol^{-1} for the least stable dimer l. In other words, the magnitude of the BSSE is the largest for the displaced-parallel conformations (2.23 – 2.67 kcal mol^{-1}), the intermediate for the T-shaped conformations (1.16 – 1.35 kcal mol^{-1}), and the least for the quasilinear and linear conformations of the dimer (0.33 – 0.51 kcal mol^{-1}). This may lead to a subsequent opinion that the magnitude of the BSSE does not strictly depend on the difference energies arising due to the mismatch between the basis functions of the two isolated C_6F_6 molecules and the corresponding complexed species for which the counterpoise concept was introduced, [43a-c] but is largely controlled by the nature of the spatial arrangements (orientations) of the two C_6F_6 subunits in the equilibrium conformational geometries of the $(C_6F_6)_2$ dimer. A similar dependence of the BSSE on the

conformational space was previously sought, in which case, it was demonstrated that the BSSE could become the source of error in the evaluation of the conformational stability differences of moderate-sized molecules, such as 1,2-dimethoxyethane, and therefore, an effort must be given for the careful evaluation of such energies. [46]

To see whether the BSSE energies estimated with the M06-2X functional are trusty, we have compared in Table 2 such energies estimated with MP2 and with the eleven other DFT/DFT-D functionals, all only for the $(C_6F_6)_2$ dimer j (Fig. 1). The results indicate that the BSSE is lying closely between 0.29 and 0.36 kcal mol^{-1} for all the eleven DFT/DFT-D functionals, and its value is as large as 0.43 kcal mol^{-1} with MP2, and that these are all in close consistent with the M06-2X value of 0.38 kcal mol^{-1}. Note that the BSSE is too large relative to the uncorrected binding energy of the dimer for a given computational method. For instance, the BSSE relative to the ΔE is as large as 41.9% with HCTH, 62.5% with M06-2X, 75.4% with MP2, 136.3% with B3LYP, and 260.4% with B3LYP-D (cf. Table 2). These results indicate that the BSSE must be used with caution for complexes involving weak binding energies, consistent with the suggestions of other authors.[49] Other than this, we have also examined the effect of zero-point vibration (ZPV) on the binding energy of the $(C_6F_6)_2$ dimer j. It is found that ZPV has somehow less pronounced effect on the ΔE (compared to the BSSE), evident of the ΔE(ZPV) data summarized in Table 2.

Whatever happens, the short F···F intermolecular distance found in several conformations of the $(C_6F_6)_2$ dimer is somehow greater than twice the vDW radii of the fluorine atom $rvdW_{F+F}$, 2.92 Å (rvdW(F) = 1.46 Å[30]) for most cases, expect for those in the geometries b and h-l (cf. Fig. 1), in which cases, such distances are slightly shorter than $rvdW_{F+F}$. An examination of the crystal of C_6F_6 (ref code HFBENZ[39], also see Fig. S2 of ESI) has showed that a majority of the F···F distances are in the 2.945–3.239 Å range, in line with our above finding. Previously, Osuna and coworkers have reported a total of twenty-three F···F contacts in the eleven $(C_6F_6)_2$ dimers examined. Of these, five were shorter, and the other eighteen were greater, than $rvdW_{F+F}$.[40] A similar conclusion can be drawn of the C···F and C···C intermolecular interactions observed in the first seven conformations of the $(C_6F_6)_2$ dimer (cf. Fig. 1a-g). These results apparently give us an impression that the recommended IUPAC feature 'In a typical halogen-bonded complex Y···X–R, the interatomic distance between X (X = halogen) and the appropriate nucleophilic atom of Y tends to be less than the sum of the van der Waals radii'[3] which may be good for medium-strong interactions, but is certainly not an effective tool for searching weakly bound interactions. This has been pointed out in similar other occasions.[5]

The molecular electrostatic potential surfaces on the 0.001 a.u. isodensity contours of the *players* in an intermolecular interaction have often demonstrated giving a realistic view of the primary driving forces drawing the molecules together.[9] However, the tool seemingly is not very effective in unraveling the nature of the primary forces responsible for driving the fluorine atoms to form the F···F intermolecular interactions. This is doubtlessly due to the fact that the electrostatic potentials on the surfaces of the covalently bound fluorine atoms in the C_6F_6 monomers are completely negative. In the recent past, Swart et al.[38a] and Varadwaj et al.[38b] have showed that this model is a sharp failure to elucidate the nature of the X···X intramolecular halogen bonding interactions in perhalogenatedethanes (CF_3–CCl_3 and CCl_3–CCl_3, e.g.) and hexahalogenated benzene derivatives, respectively. We commend that a use of this model might be inadequate to elucidate nature of the primary driving forces responsible for the attraction between the monomers in the chelates of CHF_3 and CF_4. [33e] Our view is in line with Kawai et al.[15] who have just recently demonstrated that this model is inadequate to describe the F···F interactions responsible for assembling fully fluorinated BPEPE-F18 molecules in an ordered supramolecular layered structure.

Whilst several conformers of the $(C_6F_6)_2$ dimer were examined, we have performed BHHLYP[28] level Localized Molecular Orbital Energy Decomposition Analyses (LMO-EDA) [29] only for a few specific geometries of the $(C_6F_6)_2$ dimer, h–j (cf. Fig. 1), to provide insight into the determining energetic factors bringing the totally negative fluorine atoms together. Based on this formalism, implemented in Gamess, [20b] the interaction energy of a dimer can be written as the sum of the decomposed energies arising from electrostatics (ΔE_{es}), exchange (ΔE_{ex}), repulsion (ΔE_{rep}), polarization (ΔE_{pol}), and dispersion (ΔE_{dis}). Accordingly, the computed values associated with these five components are ca. 0.15, 0.48, 0.56,–0.95, and –1.14 kcal mol^{-1} for geometry h, respectively, and are ca. 0.00, 0.37, 0.63, –0.77, –1.04 kcal mol^{-1} for geometry i, and respectively, and are ca. 0.04, 0.23. 0.37, –0.34, and –0.63 kcal mol^{-1} for geometry j, respectively, all revealing the former three components to be repulsive and the latter two attractive. These mean the F···F interactions (irrespective of their number) in each of the three geometries are stabilized mainly by polarization and dispersive forces that contribute almost equally to the binding energy. The net interaction energies for the former dimers are calculated to be ca. –0.89 and –0.81 kcal mol^{-1}, respectively, which are well along with their M06-2X SCF binding energies of –0.94 and –0.90 kcal mol^{-1}, respectively, although that calculated for the latter dimer, –0.33 kcal mol^{-1}, was found to be inequivalent with the SCF value of –0.62 kcal mol^{-1}.

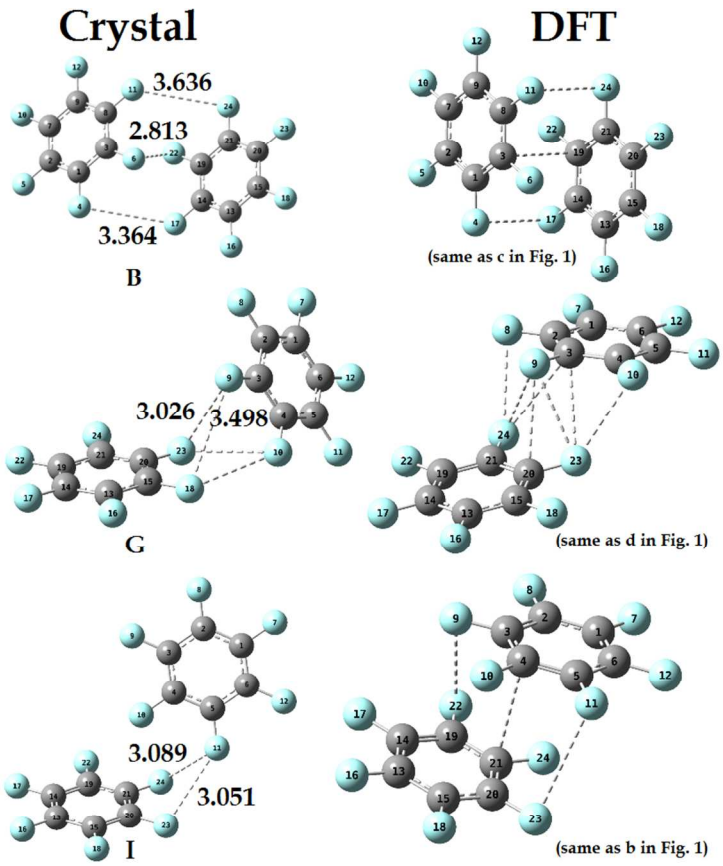

Fig. 3: Comparison of the geometries of the three symmetry non-equivalent $(C_6F_6)_2$ dimers found in the C_6F_6 crystal (ref code HFBENZ) [39] (left) with their corresponding DFT/M06-2X/6-311++G(d,p) optimized ones (right). Labeling of the dimers (B, G, and I) on the left are same as those referred in Fig. 4 of ref. 40. Selected F···F intermolecular contacts (in Å) identified in ref. 40 are illustrated; such contacts found in the optimized geometries (right) are given in Fig. 1. Atom labeling for a given system is different from the other.

The conclusions drawn above on the fidelity of the F···F intermolecular interactions are solely based on the intermolecular geometries, electrostatic surface potential extrema, and binding energies of the $(C_6F_6)_2$ dimer. However, according to Reddy and coworkers, *X···X interactions can be of several types and that it is sometimes difficult to characterize them by using geometrical criteria only*. [27a] Thus relying on their averment we have extended our analysis of chemical bonding in the $(C_6F_6)_2$ clusters, and have discussed our QTAIM[18] and RDG[19] based topological charge density results in the following section. But before that, we would specify that Osuna et al.[40] have recently analyzed eleven symmetry unique dimers of the C_6F_6 molecule synthesized in the crystalline phase.[39] In that study they could perform first principles single point MP2/aug-cc-pVDZ calculations on several crystalline geometries of the $(C_6F_6)_2$ dimer to assess their BSSE corrected binding energies ΔE(BSSE). A range of values between –0.45 and –2.65 kcal mol^{-1} was proposed for the ΔE(BSSE) in the gas phase. However, we stress that the geometries of several of these dimers in the crystalline phase when optimized in the gas phase have resulted in different geometries in the conformal space, Fig. 3. This does not overwhelm us because the geometry of the compound stabilized in the solid state does not only controlled by the static

and dynamic disorders, [47] but also influenced by several other factors, including, for example, packing forces, solvation, and counter ion effects, etc. The results manifest that the binding energies Osuna et al.[40] have reported for the $(C_6F_6)_2$ dimers might not be very meaningful.

2.2 QTAIM and RGD based topological charge density analyses

QTAIM rigorously provides the nature of an interaction in an atom-atom pair (whether covalent, coordinate, and/or ionic, etc.) in molecular compounds or in solids in terms of its unified charge density (ρ) topologies. [5,18,23,31] The theory in its simplest approach assumes a substantial accumulation of the charge density at the nucleus of an atom, represented by a (3, –3) nuclear attractor critical point (a local maximum). The critical bonding region between the two atoms in a molecule is represented by a (3, –1) bond critical point, bcp, a saddle point. At this point, the charge-density's first derivative is zero ($\nabla\rho = 0$), and its second derivative, called the Laplacian of the charge density $\nabla^2\rho$ ($\nabla^2\rho = \lambda_1 + \lambda_2 + \lambda_3$), is an extrema, where $\lambda_{i(i=1-3)}$ are the three eigenvalues of the Hessian matrix of the charge density at the bcp along the three principal directions. Thus when $\nabla^2\rho_b$ is a minimum at bcp (i.e., $\nabla^2\rho_b < 0$), we generally find a substantial concentration of the charge density at that bcp (as at the C=C and C–Cl covalent bcps in hexachlorobenzene, [31b] for example). When $\nabla^2\rho_b$ is a maximum at bcp (i.e., $\nabla^2\rho_b > 0$), we generally find a substantial depletion of the charge density at that bcp (as at the O···H intermolecular bcps in water (H_2O) clusters[31c]). However, for polar covalent bonds, $\nabla^2\rho_b$ at the bcps are positive, viz. the SO bond in SF_4O, for example.[31j] Note that for isolated chemical systems, such as 1-12-Difluorobenzo[c]phenantherene, a pair of two additional (3, –1) ring and (3, –3) cage critical points generally appears. In such cases, the Poincaré-Hopf relationship, n(ncp) + n(nncp) – n(bcp) + n(rcp) – n(ccp) = 1, a fundamental theorem of topology,[35a] is satisfied, where ncp, nncp, bcp, rcp, and ccp are the (3, –3) nuclear attractor critical point, (3, –3) non-nuclear attractor critical point, (3, –1) bond critical point, (3, +1) ring critical point, and (3, +3) cage critical point, respectively, and n refers to the number.[32b,35b,c]

According to QTAIM, the atomic basins linking each other with lines are preferential bond paths of maximal charge density, [18,31d] which are possible indicators of the presence of chemical bonding interactions. These bond paths have also been viewed as maximal exchange-correlation energy channels between bonded atomic basins according to Pendás and coworkers, [32a] and others, [32b] uncovered using Interacting Quantum Atom (IQA) model.[32c-d]

In contrary, Johnson et al.,[19a] and Contreras-García et al.,[19b-c] have recently proposed a charge density based approach, called Reduced Density Gradient (RDG), for characterizing noncovalent, coordination, and steric interactions, including halogen bonding, hydrogen bonding, σ_{hole} bonding, polar–π interactions, aromatic-aromatic (π stacking), cation–π, and metal-ligand interactions, etc. [19,33] The RDG s is a dimensionless quantity within the generalized gradient approximation of exchange-correlation term in DFT Hamiltonians,[34] and is given by Eqn. 1.

$$s = \frac{1}{[2(3\pi^2)^{\frac{1}{3}}]} \frac{|\nabla\rho|}{\rho^{\frac{4}{3}}} \quad \text{.....(1)}$$

This Eqn. envisages that as one goes far from the nuclei of a system, s will have larger values in regions where $\rho(r)$ decays to zero exponentially, and where the $\rho(r)^{4/3}$ term tends to zero more faster than the $|\nabla\rho(r)|$ term does. At the bond critical point between two bonded atomic basins in compounds, we have $|\nabla\rho(r)| = 0$, and whence Eqn. 1 gives rise

to s = 0 (the lower bound of RDG). Unequivocally, bcp is the point where one finds no difference between QTAIM and RDG.

According to Johnson et al., [19a] the supposedly stabilizing and destabilizing interactions between interatomic regions in molecules/complexes can be easy discriminated in terms of the RDG isosurface critical point, where ρ is dominated by specific noncovalent interaction (NCI), and where its gradient is nonvanishing. This critical point is a region of space characterized by either the negative or the positive sign of the second eigenvalue λ_2 ($\lambda_1 \leq \lambda_2 \leq \lambda_3$) of the Hessian matrix of the charge density. That is to say, for supposedly stabilizing interactions, $\lambda_2 < 0$, and for supposedly destabilizing interactions, $\lambda_2 > 0$, and the value of ρ determines the strength of the interaction involved. Important details on the ambiguity/unambiguity of the results of the RDG method have been discussed elsewhere.[5a-c,19, 33]

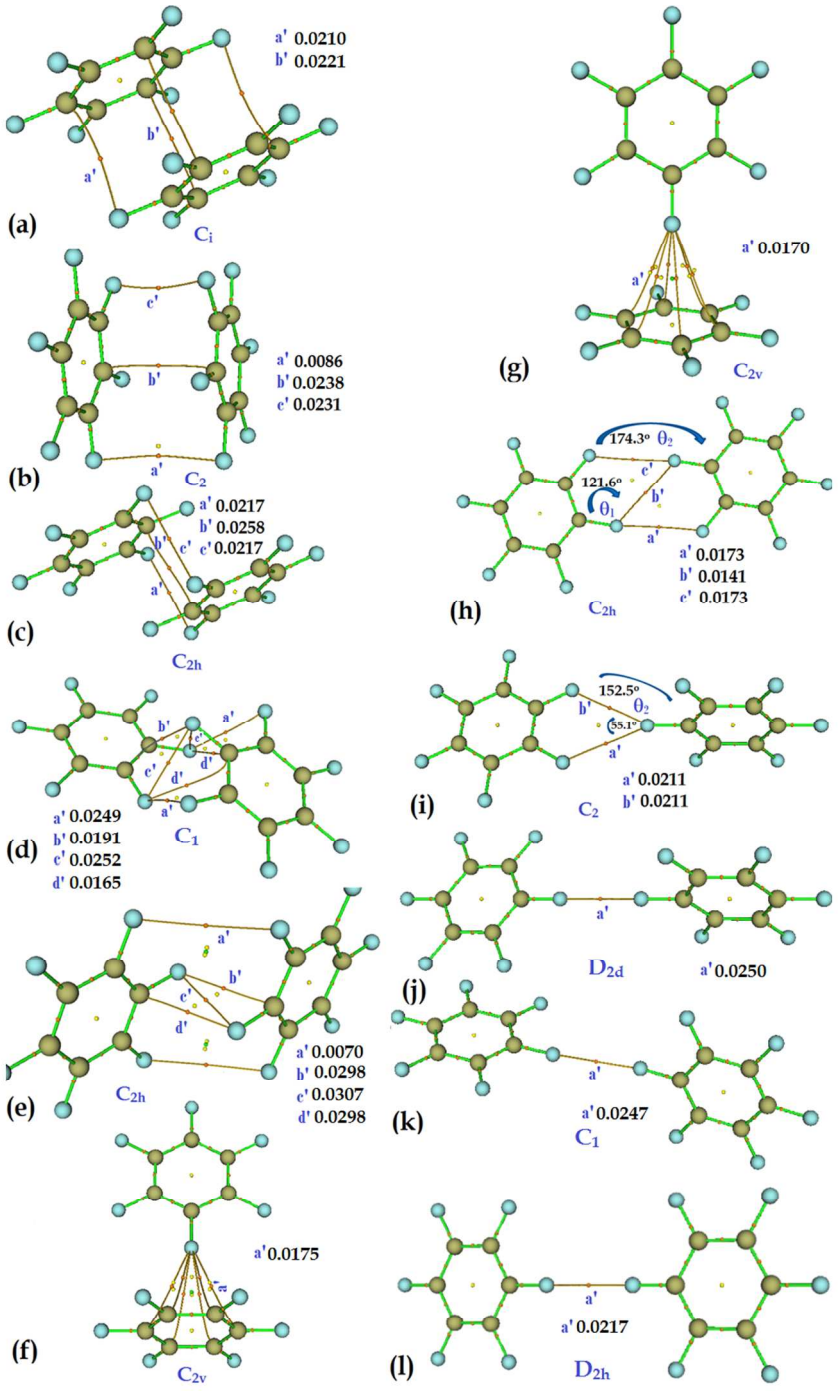

Fig. 4: Molecular graphs of the twelve conformations of the $(C_6F_6)_2$ dimer, obtained using M06-2X/6-311++G(d,p). Values of the delocalization index are listed for some selected atom pairs (in some cases, only average values are listed, viz. g), obtained within the framework of QTAIM. [36] The (3, –1) and (3, +1) bond and ring critical points are shown as tiny spheres in red and yellow, respectively. The (3, +3) critical point is shown in geen only for a few cases to avoid complications. Bond paths represent to covalent and noncovalent interactions are displayed as lines in green and dark-orange, respectively. Carbon and fluorine atoms are shown as balls in dark goldenrod and light sky blue, respectively.

Fig. 4 collects the M06-2X/6-311++G(d,p) QTAIM molecular graphs for all the $(C_6F_6)_2$ dimers examined. In the most stable dimer, Fig. 4a, we mark four intermolecular bond paths, two C···F and two C···C. These bond paths are strained (bent), and are seemingly responsible holding the two monomers together in the dimer configuration. The ρ_b values at the C···F and C···C bcps are as small as 0.0064 and 0.0089 a.u., respectively, which are comparable with those previously reported for various other noncovalently bonded interactions, such as H-bonds ($\rho_b \approx$ 0.0038 – 0.0325 a.u.), [31g] H—H bonds ($\rho_b \approx$ 0.0080 – 0.0168 a.u.),[31f] C···O bonds ($\rho_b \approx$ 0.0018 – 0.0029 a.u.),[5a] C···C bonds ($\rho_b \approx$ 0.0021 – 0.0034 a.u.),[5a] and F···F bonds ($\rho_b \approx$ 0.0080 – 0.0223 a.u.).[31a, e] The very small magnitude of ρ_b for the C···F and C···C bcps is indicative of the presence of closed-shell interactions. [5,18,23,31] The result is in concordance with the RDG

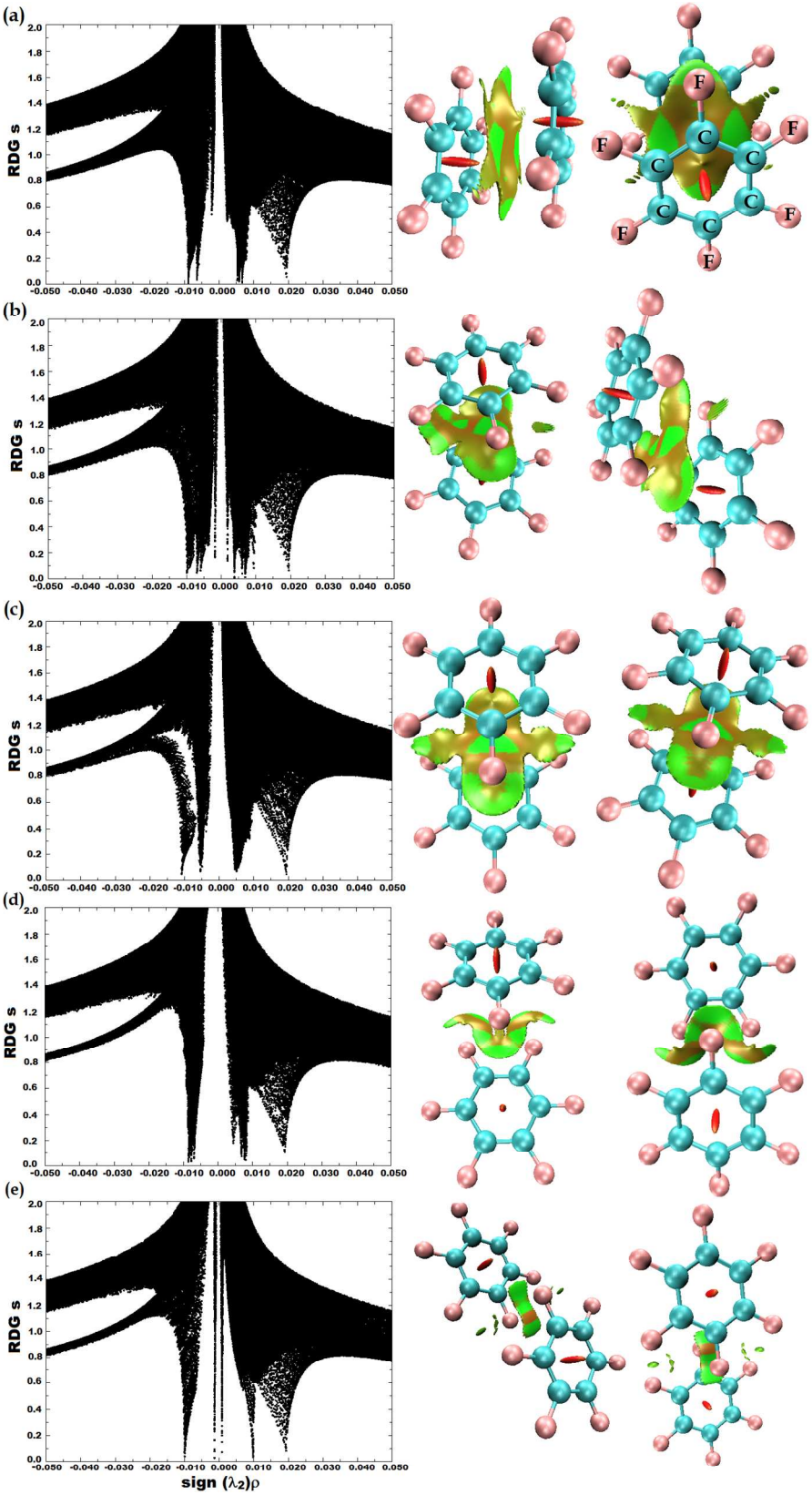

Fig. 5: M06-2X/6-311++G(d,p) calculated RDG s vs. sign(λ_2)×ρ (in a.u.) plots (left) for the first five most stable dimers of the C_6F_6 molecule (see Fig. 1**a-c**). The spikes in the sign(λ_2)×ρ < 0 and sign(λ_2)×ρ > 0 regions represent to the attractive and repulsive interactions, respectively. The s = 0.6 a.u. RDG isosurfaces in the ball and stick models representing to the former and latter interactions are painted in green and (brown) red, respectively (right). See Fig. 4a-e for comparision with the corresponding QTAIM molecular graphs.

based NCI spike and isosurface plots displayed in Fig. 5a for the corresponding dimer. As expected, it shows four attractive regions painted in green. A pair of two such regions is emanated between the four fluorine atoms, and the other pair is emanated between the four carbon atoms, both common to the two aromatic rings.

The RDG isosurface critical point features are concordant with the RDG spikes in the s vs. sign (λ_2)×ρ plot. This is not very surprising because, as expected, the λ_2 < 0 region mnemonic of stabilization unmasks two separate vertical spikes for the dimer, one for C···C and one for C···F. Similarly, the λ_2 > 0 region mnemonic of destabilization unmasks two other vertical spikes, one appears due to the (3, +1) rcps of the two aromatic rings, and one appears due to the repulsion between the two aromatic ring surfaces of the $(C_6F_6)_2$ dimer at its equilibrium geometry. These two repulsive aspects of chemical interaction are painted as red and brown RDG isosurfaces, respectively, see Fig. 5a. A similar comparative argument can also be made between the molecular and RDG graphs obtained for each of the four other dimers displayed in Figs. 4b-e and 5b-e, respectively. That said, there have been suggestions that the displaced-parallel arrangement between the two aromatic rings in dimers of similar varieties is a consequence of π—π stacking.[37] Interestingly, this is not true for the $(C_6F_6)_2$ dimers shown in Fig. 5a-e, as the

attraction between the monomers in these dimers is predominantly atom-atom/atom-bond centered, evident of the discrete RDG isosurfaces in green appearing between the interacting atomic basins. In addition, neither QTAIM nor RDG does exaggerate any type of attraction between the monomers in the $(C_6F_6)_2$ dimers that can be viewed as an eventual consequence of the alignment between the regions of positive and negative electrostatic potential, as often suggested. [37e]

The consistency between QTAIM and RDG based NCI topologies of the charge density discussed above is not quite flabbergasting.[33e] However, it is to be pointed out that the discrepancy between the results of the two methods arises, but not always, especially when the π—π interaction is the key outset of complex stabilization, as well as when the intra- and/or inter-molecular bonding region is significantly flat. To make the point more distinct, let us compare the QTAIM molecular graphs in Figs. 4b and c with the corresponding RDG isosurface graphs displayed in Fig. 5b and c, respectively. As might be immediately noticed from each of the former two graphs, QTAIM predicts three bond paths between the two C_6F_6 subunits, annunciating the possibilities of two F···F and one C···C intermolecular bonding interactions. The ρ_b and $\nabla\rho_b$ values at the bcps of such interactions in Fig. 4b are ca. 0.0071 and 0.0362 a.u., 0.0019 and 0.0121 a.u., and 0.0100 and 0.0304 a.u., respectively, while those in Fig. 4c are ca. 0.0055 and 0.0079 a.u., 0.0055 and 0.0079 a.u., and 0.0108 and 0.0337 a.u., respectively, giving the indication of the presence of closed-shell interactions.[5,31,32] Encouragingly, these links in Figs. 4b and c are indeed unraveled by NCI plots, which appear as green isosurfaces in low RDG regions between the noncovalently bonded atoms in Figs. 5b and c, respectively. In addition to

these interactions, RDG predicts a few more regions of attraction appearing between the C=C π-framework of the aromatic ring in one monomer and the fluorine's lateral negative portion in the other in both the dimers, which are absent in the corresponding QTAIM predicted molecular graphs. Again, this oddity is not very uncommon because, as discussed separately by Pendás et al.[32a] and Tognetti et al.,[44] the presence or absence of bond paths between atomic basins in molecules are directly related to the competition between the primary and secondary exchange energy channels. Specifically, when no competition is present between the exchange channels, the bond path appears, and when it is present, the bond path disappears. Similarly, the bcp between the bonded atomic basins appears when the primary exchange energy channel is dominating, and disappears when the secondary exchange energy channel is more competing.[44]

Moreover, the RDG isosurfaces for the two T-shaped configurations of the $(C_6F_6)_2$ dimer, Figs. 6a and b, apprise good consistency with the QTAIM-based molecular graphs for the corresponding species, Figs. 4f and g, respectively. The latter method demonstrates

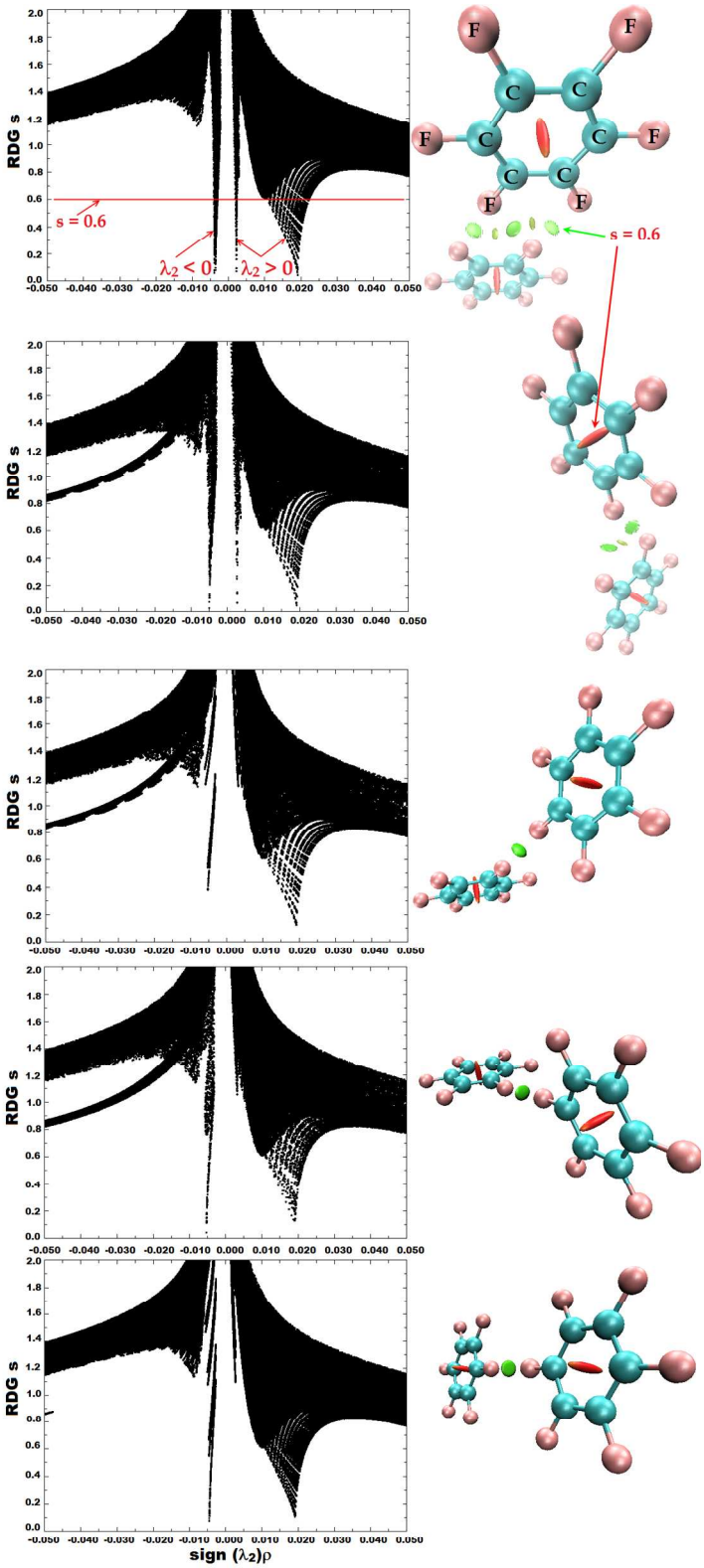

Fig. 7: M06-2X/6-311++G(d,p) level RDG s versus sign(λ_2)×ρ plots for the five high energy (least-stable) dimers (values in a.u.), see Fig. 1h-l. The spikes in the $\lambda_2 < 0$ and $\lambda_2 > 0$ regions represent to the weakly attractive and strongly repulsive regions, respectively. Shown on the right of each of these plots is the s = 0.6 a.u. RDG isosurface (ball and stick models). For each case, two different views are presented for clarification. Colored isosurfaces in green and red represent to attraction and repulsion, respectively.

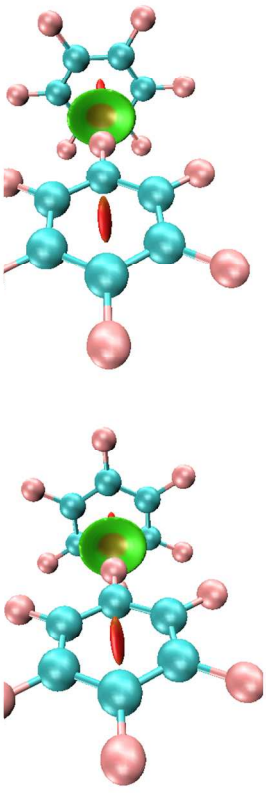

o T-shaped $(C_6F_6)_2$ dimers
kly attractive and strongly
ó a.u. RDG isosurface (ball
ed for each dimer. Colored
ely. See Figs. **1g** and **h** for

the formation of the T-shaped arrangement to be due to the attraction between the fluorine's σ_{hole} in the top monomer and each of the six carbon atoms of the bottom monomer, see Fig. 4g for example. There are therefore six bond paths and six bcps in the intermolecular bonding regions, forming a cone-like topology. ρ_b at each C···F bcp is ca. 0.0060 and 0.0059 a.u. in 4f and g, respectively, showing a depleted electron density profile at the bond critical point region. Similar bonding modes were previously identified for other systems, e.g., Ti bonding to the hydrocarbon frameworks, cyclopentadienyl, for example.[31h] According to Bader et al., [31h] an interaction of this type can be well described as a bonded cone-of-density rather than represented in terms of individual atom-atom interaction. The suggestion is perfectly in line with the RDG plots displayed in Figs. 6a and b for the corresponding dimers, respectively, in which, the interaction between the fluorine and the entire C=C π-framework of the aromatic ring can be realized in terms of a cone-of-density-like isosurface. Note that the RDG isosurface between the π_{hole} (+) and the σ_{hole} (–) regions in each of these dimers is repulsive, reminiscent of the brownish circular volumes. This is in sharp disagreement with the MESP model that characterizes the interaction between fluorine and C=C π-framework as $\pi_{hole}(+)\cdots\sigma_{hole}(-)$ type. The obvious discrepancy between the results of the two computational methodologies is indeed due to the latter in which the NCI isosurfaces resulting from the low RDG regions are very much vaguer near at the (3,+1) rcps than those near at the (3,–1) bcps.[33f] According to Johnson et al.[19a] and Contreras-García et al.,[19b-c] the RDG at the former cp is always sterically repulsive. As is so, this must then mean the RDG isosurface associated with the π_{hole} of an aromatic ring will always be repulsive regardless of whether the electrostatic surface potential associated it is purely negative, or is purely positive, which, to our view, is certainly meaningless. We believe this is probably the reason that makes us no wonder why the slipped-parallel and/or T-shaped arrangements between the two C_6F_6 subunits in the $(C_6F_6)_2$ dimers produce brownish/reddish RDG domains in the midway between the two (3,+1) rcps, see Figs. 5 and 6, for examples. These results further demonstrate that the RDG reprehensibly identifies nonbonded attractions as repulsive at longer intermolecular distances, and indeed this is not in decent agreement with the previous suggestion *repulsive interactions are only recognized as such by NCI when the repulsion is very strong.*[33e]

Fig. 7 lists the NCI plots for all the other five least stable $(C_6F_6)_2$ dimers. QTAIM molecular graphs for the corresponding dimers are given in Fig. 4 from h to l. A close examination of the latter graphs indicate the presence of three F···F bonded interactions in Fig. 4h, two in Fig. 4i, and one in each of the latter three geometries in Figs. 4j-l, all inferred from the signatures of the bond path and critical point topologies. [5, 18, 23, 31] The mean charge densities at the F···F bcps are ca. 0.0058, 0.0038, 0.0053, 0.0052, and 0.0045 a.u. for the corresponding dimers, respectively (see Table S1 for the entire detail of the topological properties). Intriguingly, these bonding modes are also palpable of the plots in Fig. 7, in which, each F···F pair is accompanied with a single disk-like circular RDG volume in green in the isosurface plot, and an RDG spike in the NCI plot in the $\lambda_2 < 0$ region, both evocative of attraction.

Cormanich and coworkers have recently demonstrated that the RDG results are not always unambiguous because they unpleasantly identify nonbonded attractions as repulsive at short interatomic distances (as in CX_4 dimers, for example), and the interactions that are attractive with it do not translate into noticeable energetic stabilization. [33e] The latter characteristic can also be acknowledged from the results of this study. For example, the (stability) trend in the binding energies of the first five $(C_6F_6)_2$ dimers listed in Fig. 1 is a > b > c > d > e (see Table 1 for ΔE values). This is not sharply in consistent with the corresponding trend reflected in the vertical sizes of the RDG spike, as well as that in the peak positions of such spikes below s = 0.6 a.u. in the $\lambda_2 < 0$ region for the corresponding dimers (passing from Figs. 5a to 5e). A similar conclusion can also be released comparing the trend in the binding energies of the three F···F bonded

$(C_6F_6)_2$ dimers passing from Fig. 1j to 1l against that in their corresponding RDG spike sizes, as well as that in the peak positions of such spikes below the s = 0.6 a.u. line in red in the $\lambda_2 < 0$ region passing from Fig. 7a to 7c.

From the data in Table S1, it is unambiguous that the three eigenvalues of the Hessian of the charge density matrix are such that for all F···F/C···F/C···C bcps $\lambda_1 < 0$, $\lambda_2 < 0$, and $\lambda_3 > 0$. Because the magnitude of λ_3 is too large compared to the other two eigenvalues for these bcps, the Laplacian of the charge density, which is the mathematical sum of these three eigenvalues $\lambda_{i(i=1-3)}$ ($\nabla^2\rho_b = \lambda_1 + \lambda_2 + \lambda_3$), is positive at all such bcps, with $\nabla^2\rho_b$ values varying in the 0.0050 – 0.0492 a.u. range. Notable from Table S1 are also the kinetic energy densities (G_b) at the F···F/C···F/C···C bcps that are larger than their corresponding potential energy densities (V_b), resulting in positive total energy densities ($H_b = (V_b + G_b) > 0$) at those bcps. The diagnostics $\nabla^2\rho_b > 0$ and $H_b > 0$ synchronous with the F···F/C···F/C···C bcps are qualifications of closed-shell interactions.[5, 18, 23]

The QTAIM and RDG characterized noncovalently bonded interactions in the conformations of the $(C_6F_6)_2$ dimer are further confirmed by the analysis of the QTAIM-based delocalization index (DI), a two-electron property that has long been viewed as a measure of bond order. [36] By definition,[51] this property can be calculated for any atomic pairs regardless of whether the atoms in molecules are bonded to each other or not (i.e., whether there exist bond paths in the bonded atomic basin pairs or not). As summarized in Table S1, the DIs calculated for all the F···F, C···F, and C···C bonding interactions are in the narrow range between 0.0070 and 0.0307, which are comparable with the magnitudes previously reported for similar C···C/C···O bonded noncovalent interactions.[5a] Even so, this range is incomparable with those reported for the F···F intramolecular bonding interactions found in several polyfluoro-substituted aromatic compounds (values between 0.0374 and 0.0902), as the large DI values were predicted for very short F···F inter-nuclear separation distances ranged between 2.3 and 2.8 Å. [31a]

Now, let us look at Fig. 4a. It is apparent from this that except for the two well defined F···F interactions QTAIM's bond path and critical point topologies do not reveal the possibility of any other intermolecular bonding interactions between the other fluorine atoms in the dimer. However, the NCI plot of this the dimer in Fig. 5a gives an indication of the presence of four new F···F interactions of type-Ic. Although these interactions are too weak, they can be readily evident of the dot-like multiform domains between the fluorine atoms painted in colors ranging from light brown to green, characterized by the $F_{13}\cdots F_{20}$ (3.383 Å), $F_{15}\cdots F_{22}$ (3.382

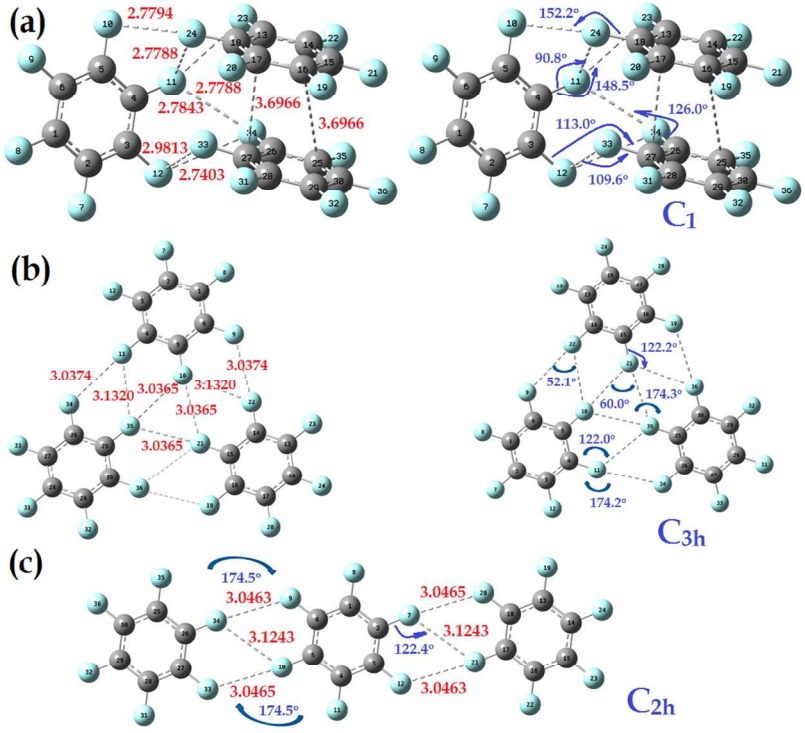

Fig. 8: The three ptimized geometries of the $(C_6F_6)_3$ trimer, obtained with M06-2X/6-311++G(d,p). Values of selected intermolecular contact distances (in Å) and bond angles (in °) are shown. For clarity, two geometries are illustrated for each of a) and b), one summarizes the intermolecular contact distances and the other the important bond angles.

Å), $F_{16}\cdots F_{23}$ (3.383 Å), and $F_{18}\cdots F_{19}$ (3.382 Å) interactions (see Fig. 1a for atom labeling). A DI value of 0.0073 is estimated for each of the four F···F pairs, giving an indication that these are all representatives of attraction.

2.3 Trimers and tetramers of C_6F_6

A specific aim of this section was to show whether the recently endorsed[15] inverted windmill geometry between the fluorine atoms in the two-dimensional supramolecular layered structure formed of the fully fluorinated BPEPE-F18 molecules is implicative of the clusters the C_6F_6 molecules. And whether such clusters are denouement of cooperative binding. In order to provide reasonable answers to these two questions, a few geometries of the conformations of the $(C_6F_6)_n$ (n = 3, 4) clusters were fully energy-minimized with M06-2X/6-311++G(d,p).

Figs. 8 and 9 illustrate the optimized geometries of the three conformations of the $(C_6F_6)_3$ trimer and of the two conformations of the $(C_6F_6)_4$ tetramer, respectively. As can be apparently seen from Fig. 8c/9b, the planar array of the three/four subunits of the C_6F_6 molecule results in the formation of a C_{2h} geometry for the $(C_6F_6)_3/(C_6F_6)_4$ trimer/tetramer. However, when such subunits are planerly non-arrayed, they produce geometries illustrated in Figs. 8a-b and 9a. Except for the geometry in Fig. 8a, the fluorine atoms in all the above four cases are mainly linked with each other via type-Ia and -II intermolecular topologies, Scheme 1, comparable with that found for the $(C_6F_6)_2$ dimer h (Fig. 4). Interestingly enough, the geometry in Fig. 8b, as well as that in Fig. 9a, includes windmill type geometry between the fluorine atoms, which is analogous to that reported in ref. 15. This kind of geometrical arrangement between the C_6F_6 subunits in $(C_6F_6)_3/(C_6F_6)_4$ is indeed a consequence of attraction between the merely negative fluorine atoms, arising mainly due to the polarization and dispersion forces, wherein electrostatics plays an important role in determining the repulsive part of the interaction (*vide supra*). It is worth mentioning that Kawai et al.[15] were not the first, but Reddy et al.[27a] were also observed similar windmill type intermolecular topologies between the halogen atoms when fully halogenated aromatic compounds were self-assembled in the solid state, with the halogens were notably of the chlorine, bromine, and iodine atoms.

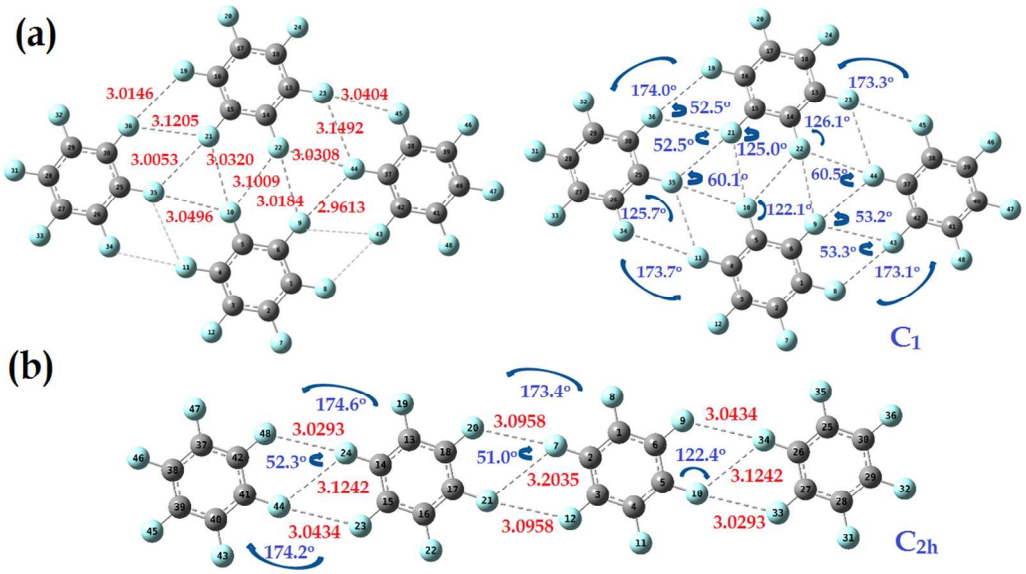

Fig. 9: Optimized geometries of the $(C_6F_6)_4$ tetramer, obtained with M06-2X/6-311++G(d,p). Values of selected intermolecular contact distances (in Å) and bond angles (in °) are shown. For clarity, two geometries are presented for a), one summarizes the intermolecular contact distances and the other the important bond angles.

Whether the intermolecular bonding topologies between the fluorine atoms in the geometries of the $(C_6F_6)_n$ (n = 3, 4) clusters are persuasive of attraction (closed-shell type) are inferred examining their QTAIM based molecular graphs (Fig. 10) and topological properties of the charge density (Tables S2 and S3). As can be seen from the molecular graphs, the nuclei of the bonded fluorine atoms in the F···F pairs of these clusters are evidenced by the presence of the bond

path and (3, −1) bcp topologies. The charge density at such bcps is very small, all between 0.0033 and 0.0100 a.u. for the trimers, and that between 0.0027 and 0.0045 a.u. for the tetramers. The signs and magnitudes of $\nabla^2\rho_b$ and H_b at such bcps are positive and small (cf. Tables S2 and S3 for values), revealing qualifications of closed-shell interactions. The QTAIM based delocalization indices for the F···F pairs are computed to lie between 0.0132 and 0.0315 for the trimers, and are between 0.0110 and 0.0167 for the tetramers (see detailed values in Fig. 9), which both are comparable with the corresponding values of similar contacts in the $(C_6F_6)_2$ dimers illustrated in Fig. 4. All these signatures of noncovalent bonding interactions are in fair agreement with the RDG-based spike and isosurface plots illustrated in Figs. S3 and 11 for the trimers and tetramers of the C_6F_6 molecule, respectively. To be more explicit, these latter plots each reveals expected green isosurfaces, as well as the vertical spikes, in the $\lambda_2 < 0$ region at low RDG, which are suggestive of F···F bonding interactions. A similar conclusion might also be drawn for the C···C and C···F interactions of the conformation illustrated in Fig. 8a (see Table S2 for a detailed topological properties and 10a for molecular graph).

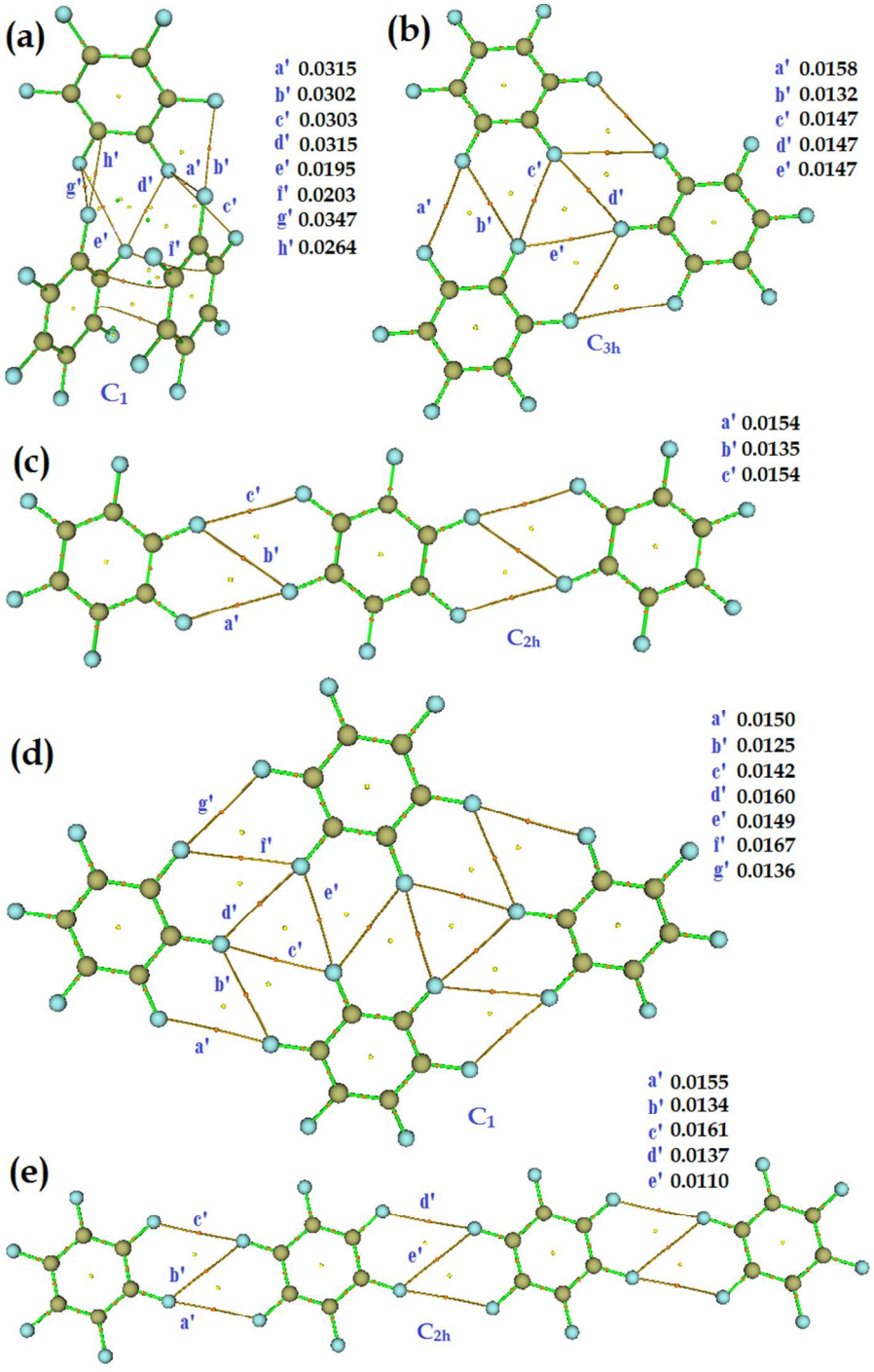

Fig. 10: Molecular graphs for some selected conformations of the $(C_6F_6)_n$ (n = 3, 4) clusters, obtained using M06-2X/6-311++G(d,p). Values of delocalization index DI are listed for selected atom pairs, obtained within the framework of QTAIM. [36] The (3, −1) and (3, +1) bond and ring critical points are shown as tiny spheres in red and yellow, respectively. The (3, +3) cage critical point is shown in green only for a few cases to avoid complications. Bond paths represent to covalent and noncovalent bonds are displayed as lines in green and dark-orange, respectively. Carbon and fluorine atoms are shown as balls in dark goldenrod and light sky blue, respectively. See Figs. 8 and 9 for details of atom numbering.

The fluorine in the conformations of the $(C_6F_6)_2$ dimer serves as bi-, tri-, or tetra-furcating centers for F···F bond formations, Fig. 4. The particular theme is persistent with the same atom in the conformations of the $(C_6F_6)_3$ trimer and of the $(C_6F_6)_4$ tetramer. These are apparent from the QTAIM molecular graphs illustrated in 10b-e, wherein the fluorine divulges its capacity to act as tri- and tetra-furcated centers for the F···F bond formations. In the $(C_6F_6)_3$ trimer, Fig. 10a, it smartly plays its role as di-, tri-, and tetra-furcating centers. In all the above

cases, it is functioning both as an electrophile and as a nucleophile for the F···F pair formation. Although the calculated F···F bond lengths and ∠F···F–C bond angles in the $(C_6F_6)_{n\ (n\ =\ 3,\ 4)}$ clusters in Figs. 10b-e are almost identical to those found in the geometry of the $(C_6F_6)_2$ dimer h (Fig. 4), it is eloquent that the F···F interactions marked b' are formed due to the overlapping of fluorine's negative lateral regions of identical electrostatic surface potential ($V_{s,max}$ = –6.5 kcal mol^{-1} for each, Fig. 2).

But now the question arises: what then compels the completely negative fluorine atom(s) in a C_6F_6 monomer to attract the same atom(s) in another monomer(s) at the equilibrium geometries of the $(C_6F_6)_n$ (n = 2,3,4) clusters. As

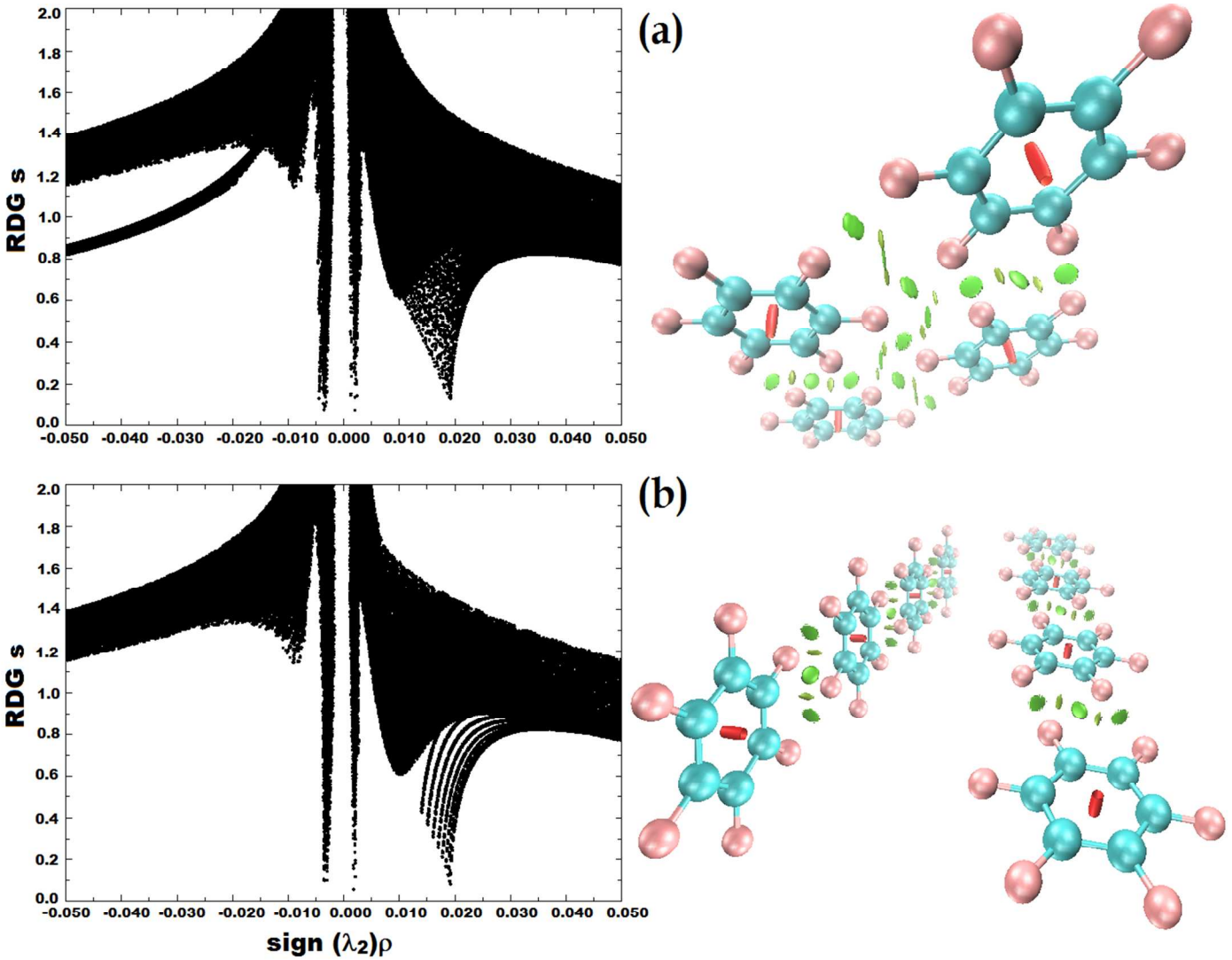

Fig. 11: RDG s vs. sign(λ_2)×ρ (in a.u.) plots for the two selected tetramers of the C_6F_6 molecule, obtained with M06-2X/6-311++G(d,p). The spikes in the sign(λ_2)×ρ < 0 and sign(λ_2)×ρ > 0 regions represent to the stabilizing and destabilizing interactions, respectively. The s = 0.6 a.u. RDG isosurfaces in the ball and stick models representing to the former and latter interactions are painted in green and red, respectively. Two different views of the isosurface of (a) are presented for clarity. See Fig. 9 for geometric details, and Fig. 10d-e for the QTAIM based molecular graphs for comparision.

discussed already above, the MESP model does not provide any straightforward answer to this question because it does not allow attraction between the two negative sites. The LMO-EDA model explains polarization and dispersion to be the main driving forces bringing the two C_6F_6 monomers together in the equilibrium cluster geometries. QTAIM's bond path topology demonstrates that the fluorine atoms in C_6F_6 would serve both as F-bond acceptor and donor for the formation of the F···F pairs in the $(C_6F_6)_n$ (n = 2,3,4) clusters. The latter two conclusions are in sharp contrast with Vallejos et al. who have suggested that the fluorine atoms are not generally polarizable and therefore not typically considered X-bond donors.[8e] Nonetheless, to provide more insight into factors that explain why the similarly negatively charged fluorine atoms in C_6F_6 are capable of forming the F···F bonding interactions, we have extended our study to perform QTAIM based source function analysis for some selected $(C_6F_6)_n$ clusters, including those illustrated in Figs. 4h, 4j-l, 8b-c, and 9a. For the geometry in Fig. 4h, each fluorine sharing the F···F interaction contributes a negative ρ value of –0.0032 (–

90.0%) a.u. to each of its two equivalent bcps marked a' and c', and of −0.0030 (−76.5%) a.u. to the bcp marked b'. Similarly, each fluorine contributes a negative ρ value of −0.0026 (−57.4%) a.u. to the $F_{16}\cdots F_8$ bcp in Fig. 4j (see Fig. 1j for atom numbering), of −0.0023 (−44.2%) a.u. to the same bcp in Fig. 4k, and of −0.0024 (−45.1%) a.u. to the same bcp in Fig. 4l. For the geometry in Fig. 8c, the fluorine atoms contribute negative ρ values of −0.0031 (−90.7%) and −0.0032 (−98.0%) a.u. to the $F_9\cdots F_{34}$ and $F_{34}\cdots F_{10}$ bcps, respectively. For the geometry in Fig. 8b, the fluorine atoms in $F_9\cdots F_{22}$, $F_{22}\cdots F_{10}$, and $F_{10}\cdots F_{21}$ contribute negative ρ values of −0.0031 (−85.8%), −0.0032 (−90.6%), and −0.0033 (−87.6%) a.u. to the respective bcps. And, similarly, the fluorine atoms in the geometry in Fig. 9a contribute negative ρ values of −0.0030 (−87.0%), −0.0033 (−105.3%), −0.0032 (−92.9%), −0.0032 (−88.6%), and −0.0032 (−92.3%) to the $F_{45}\cdots F_{23}$, $F_{23}\cdots F_{44}$, $F_{22}\cdots F_{10}$, $F_{22}\cdots F_9$, and $F_{22}\cdots F_{44}$ bcps, respectively. Our above observation is in line with Eskandari et al., [12e] who have recently concluded that in fluorine-centered noncovalent interactions the fluorine has the tendency to serve as a sink of charge density for the N···F bcps.

Whether or not the fluorine atoms of the C_6F_6 monomers in the $(C_6F_6)_{n\ (n\ =\ 3,\ 4)}$ trimers/tetramers are bonded to each other are confirmed by estimating the uncorrected binding energies ΔE of these clusters. For this reason, we have used the relation: ΔE(trimer/tetramer) = E(trimer/tetramer) − [E(dimer/trimer) + E(C_6F_6)], where E refers to the total electronic energy of the molecular unit/subunit involved. The estimated ΔE values for the $(C_6F_6)_3$ trimers in Figs. 8c and b are ca. −1.89 and −2.76 kcal mol^{-1}, respectively, with the former is about −0.87 kcal mol^{-1} less stable than the latter one. The tendency is perpetual passing from the $(C_6F_6)_3$ trimer to the $(C_6F_6)_4$ tetramer. For instance, the ΔE for the $(C_6F_6)_4$ tetramers in Figs. 9b and a are ca. −2.81 and −4.49 kcal mol^{-1}, respectively, with the former is about −1.68 kcal mol^{-1} less stable than the latter. These results suggest that the ΔE values estimated for the planar arrayed and non-arrayed $(C_6F_6)_4$ tetramers are larger than those found for the corresponding conformations of the $(C_6F_6)_3$ trimer. And, compared to the $(C_6F_6)_2$ dimer h (Fig. 1), which has intermolecular topologies similar to those of 8b-c and 9a-b, the affinity of binding between the monomers in the $(C_6F_6)_3$ trimers, as well as in the $(C_6F_6)_4$ tetramers, increases.

The above results also indicate that the C_6F_6 subunits forming the planar arrayed geometries are relatively less stable than the corresponding planar non-arrayed ones, which is regardless of the nature of the cluster types examined. The characteristic is perspicaciously justified because the F···F intermolecular contact distances commenced between the fluorine atoms in the latter arrangement are larger in number and more tightly packed than those in the former arrangement. For example, the $(C_6F_6)_3$ geometry in Fig. 8c comprises of six F···F pairs (F···F distances vary between 3.0463 and 3.1234 Å), while that in Fig. 8b comprises of nine such pairs (F···F distances vary between 3.0374 and 3.0365 Å), which are relatively shorter. Similarly, the planarly arrayed and non-arrayed $(C_6F_6)_4$ tetramers comprise of nine and fourteen F···F pairs, respectively, with the contacts in the former species are somehow loosely bound (cf. Fig. 8). This characteristic might explain why Kawai et al.[15] were able to observe an analogous planarly non-arrayed supramolecular layered structure formed of the BPEPE-F18 molecules on the Ag(111) surface. In any event, we have energy-minimized yet another conformation for the $(C_6F_6)_3$ trimer, Fig. 8a. Surprisingly, its binding energy is about 4.4 times larger than its other conformation in Fig. 8b (values of ΔE ≈ −12.11 vs. −2.76 kcal mol^{-1}), perhaps giving some evidence of the presence of synergistic binding. Such an attribute is not unexpected because the geometry of this conformation consists of a network of F···F type-Ic and -II contacts. These, along with the C···F and C···C long-ranged contacts identified, are altogether responsible for the effective stabilization of the trimer.

3. Conclusion

The study represented a first detailed conformational analysis of the $(C_6F_6)_2$, and to a smaller extent, $(C_6F_6)_3$ and $(C_6F_6)_4$ clusters using density functional theory. An original goal towards this investigation was intended to display the potential capacity of the C_6F_6 molecules in forming various homomolecular dimers, trimers, and tetramers, and to see whether they can be used for the emergence of self-assembled supramolecular clusters.

We showed that the geometries of several conformations of the $(C_6F_6)_2$ dimer to be stabilized by a varied number of long-ranged contacts, involving the F···F, C···F, and C···C, and in a few cases, by the π···σ_{hole} and π···lone-pair intermolecular topologies. These were found not to have dissimilar characteristics compared to what might be expected for the halogen-, hydrogen-, and other σ_{hole} interactions.

The binding energies ΔE for all the twelve $(C_6F_6)_2$ dimeric configurations ware ranged between –0.51 to –7.38 kcal mol^{-1}.The ΔE ($\Delta E \approx$ –7.38 kcal mol^{-1}) for the most stable displaced-parallel arrangement (slipped but not stacked) was found to be roughly more than twice larger than that of the benzene dimer (–2.63 kcal mol^{-1}), and was somehow comparable with that of the indole···hexafluorobenzene[25a] (–7.18 kcal mol^{-1}) and benzene···hexafluorobenzene[25b,c] (–6.32 kcal mol^{-1}) π-stacked dimers. The BSSE was found to have significant effect on the nature of the conformational geometry, thus on magnitude of the ΔE.

Of significant interest was to explore the equilibrium geometries of a few of the homomolecular dimers, trimers, and tetramers of the C_6F_6 the molecule stabilized by the C–F···F–C intermolecular topologies, and which have significant geometrical similarities with the self-assembled supramolecular layered structure formed of the BPEPE-F18 molecules. Indeed, several such geometries between the C_6F_6 monomers were identified for the dimers, trimers, and tetramers. However, two geometries forming the pseudo windmill type topologies comprising of the C–F···F–C interactions were the planar $(C_6F_6)_3$ trimer (C_{3h}) and the nearly planar $(C_6F_6)_4$ tetramer (roughly C_2), in consonance with Kawai et al.'s observation.[15] Reddy et al.[27a] have also previously reported topologically similar windmill type geometries between the hexahalogenated benzene derivatives excluding the involvement of the fluorine atom.

According to Kawai et al.'s interpretation, the F···F interactions in the supramolecular layered structure formed of the BPEPE-F18 molecules were stabilized mainly by dispersion. However, our LMO-EDA results have suggested that the formation of the F···F pair in the geometries of the $(C_6F_6)_2$ dimer is a consequence of attraction caused by the polarization and dispersive forces.

The electrostatic surface potentials on the axial and equatorial portions of the covalently bound fluorine in C_6F_6 were computed to be negatively nonequivalent, authenticating the anisotropic nature of the charge density profile around its nucleus. This has led to an immediate understanding that each fluorine in C_6F_6 accompanies a negative σ_{hole} along the outer portion of the C–F σ-axis. We have therefore made it apparent in this study that the nature of the fluorine's σ_{hole} in BPEPE-F18 could be similar to the one found in C_6F_6 given the covalently bound fluorine atoms in both these two compounds are somehow geometrically complementary, an interpretation which is against what was surmised by Kawai et al.[15]

We have showed that the totally negatively charged fluorine in isolated C_6F_6 has the potential to temper engage in directional bonding interactions with the nearest negative sites localized on the surfaces of the same atoms in other C_6F_6, despite it does not have a positive σ_{hole}. The perpetual adaptability of fluorine's directional behavior was evident in several dimeric, trimeric and tetrameric geometries of the C_6F_6 molecule, however, this was not very crystal-clear in several such geometries of the clusters that involve the F···F type-Ia/type-Ic intermolecular topologies, wherein the lateral portion of the fluorine in one C_6F_6 was involved attractively with an equivalent lateral negative portion of the same

atom in other C_6F_6. Evidently, the molecular electrostatic surface potential model that was extremely useful in the past in unraveling the electrophilic and nucleophilic nature of atoms/fragments in molecules, as well as in elucidating the chemistry of noncovalent interactions, was found inadequate to provide any insightful explanation accounting for the reason why the wholly negatively charged fluorine in an isolated C_6F_6 could interact cooperatively with the same atom in another C_6F_6 to form the C–F···F–C supramolecular synthon, thereby promulgating failure of the model.

Contrariwise, the results of the QTAIM and RDG charge density based models were found to be the most remarkable. Although QTAIM, in a few instances, did not show the expected topological signatures of bonding, and RDG gave unphysical repulsive aspects of boding near the ring critical point regions, separate applications of these methodologies to the $(C_6F_6)_{n\ (n=2-4)}$ clusters could enable us confirming the attractive nature of the C–F···F–C (and other) interactions through their unified topological characteristics, reflecting superiority of these two methods over the former. Even so, QTAIM's source function analysis tool has allowed us to justify that for the formation of the F···F interactions the fluorine does not necessarily have to be a source, rather it would prefer to serve as a sink, in agreement with a recent rationale.[12e]

Finally, we would like to point out that the calculated signs and magnitudes of QTAIM charges conferred on the fluorine atoms sharing the C–$F^{\delta-}\cdots^{\delta-}$F–C interaction are identical (values approximately between –0.611 and –0.614 *e*), witnessing *like liking like*. The earmark is compatible with what was proposed some time ago for the A–H···H–B bonding interaction.[31i] To go into a little detail of this latter interaction, it has been said that this is attractive, and is formed when both the hydrogen atoms are either electrically neutral or carry small charges which are usually of similar sign, and the A–H bond upon the formation of the A–H···H–B interaction decreases. Notwithstanding, the aforementioned unequivocal signatures of noncovalent interactions supporting the reliability of the $F^{\delta-}\cdots^{\delta-}F$ interactions formed between the two equally charged species do not come along with the previous suggestion '*halogen bonding can readily be understood as the attractive interaction between the positive outer region on the halogen and the negative site*', nor do they come along with the assertion *the negative electrostatic potential associated with a* σ_{hole} *precludes the possibility of halogen bonding–unless the electric field of the negative site is strong enough to induce a positive region on the halogen*. Thus in analogy with A–H···H–B bonding interaction, we suggest referring the attractive interaction between the two fluorine atoms observed in the $(C_6F_6)_{n\ (n=2-4)}$ clusters to as *F···F (or difluoride) bonding*. It is expected that this study will help others to explore the promising and hidden noncovalent chemistry of many other fluorine-based materials.

References

1. (a) P. Auffinger, F. A. Hays, E. Westho and P. Shing Ho, *Proc. Natl. Acad. Sci. U. S. A.*, 2004, 101, 16789; (b) M. R. Scholfield, C. M. V. Zanden, M. Carter and P. Shing Ho, *Protein Science*, 22, 2013, 139; (c) R. Wilcken, M. O. Zimmermann, A. Lange, A. C. Joerger and F. M. Boeckler, *J. Med. Chem.*, 2013, 56, 1363; (d) Y. Lu, T. Shi, Y. Wang, H. Yang, X. Yan, X. Luo, H. Jiang and W. Zhu, *J. Med. Chem.*, 2009, 52, 2854; (e) A. Mukherjee, S. Tothadi and G. R. Desiraju, *Acc. Chem. Res.*, 2014, 47, 2514; (f) A. Priimagi, G. Cavallo, P. Metrangolo and G. Resnati, *Acc. Chem. Res.*, 2013, 11, 2686.
2. (a) P. Metrangolo and G. Resnati, Halogen Bonding: Fundamentals and Applications, Springer-Verlag, Berlin, Heidelberg, Germany, 2008; (b) F. Meyer and P. Dubois, *Cryst. Eng. Comm*, 2013, 15, 3058.
3. G. R. Desiraju, P. Shing Ho, L. Kloo, A. C. Legon, R. Marquardt, P. Metrangolo, P. Politzer, G. Resnati and K. Rissanen, *Pure Appl. Chem.*, 2013, 85, 1711.
4. (a) G. P. Schiemenz, *Z. Naturforsch.*, 2007, 62b, 235; (b) G. A. Jeffrey and W. Saenger, Hydrogen Bonding in Biological Structures, Springer Verlag, Berlin, 1991.

5. (a) P. R. Varadwaj, A. Varadwaj and B.-Y. Jin, *Phys. Chem. Chem. Phys.*, 2014, 16, 17238; (b) P. R. Varadwaj, A. Varadwaj and B.-Y., Jin, *Phys. Chem. Chem. Phys.*, 2014, 16, 19573; (c) A. Varadwaj, P. R. Varadwaj and B.-Y. Jin, *Int. J. Quantum Chem.*, 2015, 115, 453; (d) S. J. Grabowski, *Phys. Chem. Chem. Phys.*, 2014, 16, 1824; (e) D. A. Smith, L. Brammer, C. A. Hunter and R. N. Perutz, *J. Am. Chem. Soc.*, 2014, 136, 1288.
6. (a) J. P. M. Lommerse, A. J. Stone, R. Taylor and F. H. Allen, *J. Am. Chem. Soc.*, 1996, 118, 3108; (b) B. Bankiewicz and M. Palusiak, *Struct. Chem.*, 2013, 1297; (c) J. Wang, M. Sanchez-Rosello, J. Aceña, C. del Pozo, A. E. Sorochinsky, S. Fustero, V. A. Soloshonok and H. Liu, *Chem. Rev.*, 2014, 114, 2432.
7. (a) D. O' Hagan, *J. Fluorine Chem.*, 2010, 131, 1071; (b) V. P. Reddy, Organofluorine Compounds in Biology and Medicine, Elsevier, 2015 (ISBN: 978-0-444-53748-5).
8. (a) P. Th. van Duijnen and M. Swart, *J. Phys. Chem. A*, 1998, 102, 2399; (b) P. Schwerdtfeger, Table of experimental and calculated static dipole polarizabilities for the electronic ground states of the neutral elements (in atomic units), Last Update: February 11, 2014 (available at: http://ctcp.massey.ac.nz/Tablepol2014.pdf, and at: http://ctcp.massey.ac.nz/dipole-polarizabilities); (c) A. C. Legon, *Phys. Chem. Chem. Phys.*, 2010, 12, 7736. (d) S. A. C. McDowell and J, A. Joseph, *Phys. Chem. Chem. Phys.*, 2014, 16, 10854; (e) M. J. Vallejos, P. Auffinger and P. Shing Ho, Ch 23.6. Halogen interactions in biomolecular crystal structures, *Int. Tables Cryst. F.*, Ch. 23.6, 2012 (available at: http://www-ibmc.u-strasbg.fr/arn/Westhof/publ_West/doc2011/r2011_MVallejos_Tables.pdf).
9. (a) P. Politzer, J. S. Murray and T. Clark, *Phys. Chem. Chem. Phys.*, 2010, 12, 7748; (b) P. Politzer, J. S. Murray and T. Clark, *Phys. Chem. Chem. Phys.*, 2013, 15, 11178; (c) J. S. Murray and P. Politzer, *WIREs Comput. Mol. Sci.: Overview*, 2011, 1, 153; (d) P. Politzer and J. S. Murray, *Chem. Phys. Chem.*, 2013, 14, 278; (e) P. Politzer, J. S. Murray, G. V. Janjic and S. D. Zaric, *Crystal*, 1024, 4, 12; (f) J. S. Murray, P. Lane, T. Clark, K. E. Riley and P. Politzer, *J. Mol. Model*, 2012, 18, 541.
10. (a) P. Metrangolo, J. S. Murray, T. Pilati, P. Politzer, G. Resnati and G. Terraneo, *Cryst. Growth Des.*, 2011, 11, 4238; (b) P. Metrangolo, J. S. Murray, T. Pilati, P. Politzer, G. Resnati and G. Terraneo, *Cryst. Eng. Comm.*, 2011, 13, 6593.
11. (a) T. Brinck, J. S. Murray and P. Politzer, *Int. J. Quantum Chem.*, 1992, 44, 57; (b) T. Clark, M. Hennemann, J. S. Murray and P. Politzer, *J. Mol. Model.*, 2007 13, 291; (c) T. Clark, *WIREs Comput. Mol. Sci.*, 2013, 3, 13; (d) K. E. Riley, J. S. Murray, P. Politzer, M. C. Concha and P. Hobza, *J. Chem. Theory Comput.*, 2009, 5, 155.
12. (a) J. S. Murray, P. Lane and P. Politzer, *J. Mol. Model.*, 2009, 15, 723; (b) J. S. Murray and P. Politzer, *Croat. Chem. Acta*, 2009, 82, 267; (c) W. Li, Y. Zeng, X. Zhang, S. Zheng and L. Meng, *Phys. Chem. Chem. Phys.*, 2014, 16, 19282; (d) Y. X. Lu, J.-W. Zou, Q.-S. Yu, Y.-J. Jiang and W.-N. Zhao, *Chem. Phys. Lett.*, 2007, 449, 6; (e) K. Eskandari and M. Lesan, *Chem. Eur. J.*, 2015, 21, 4739.
13. (a) M. D. Esrafili and B. Ahmadi, *Comput. Theor. Chem.*, 2012, 997,77; (b) M. D. Esrafili MD and N. Mohammadirad, *J Mol. Model*, 2013, 19, 2559; (c) M. D. Esrafili, F. Mohammadian-Sabet and M. Solimannejad, *Struct. Chem.*, 2014, 25, 1197; (d) R. Pal, G. Nagendra, M. Samarasimhareddy, V. V. Sureshbabub and T. N. Guru Row, *Chem. Commun.*, 2015, 51, 933.
14. P. Zhou, J. Zou, F. Tian and Z. Shang, *J. Chem. Inf. Model.*, 2009, 49, 2344
15. S. Kawai, A. Sadeghi, F. Xu, L. Peng, A. Orita, J. Otera, S. Goedecker and E. Meyer, *ACS Nano*, 2015, 9, 2574.
16. (a) Y. Zhao and D. G. Truhlar, *Theor. Chem. Acc.*, 2008, 120, 215; (b) Y. Zhao and D. G. Truhlar, *Acc. Chem. Res.*, 41, 157; (c) S. Kozuch and J. M. L. Martin, *J. Chem. Theory Comput.*, 2013, 9, 1918; (d) A. Forni, S. Rendine, S. Pieraccini and M. Sironi, *J. Mol. Graphics Model.*, 2012, 38, 31; (e) E. G. Hohenstein, S. T. Chill and C. David Sherrill, *J. Chem. Theory Comput.*, 2008, 4, 1996; (f) S. Kozuch and J. M. L. Martin, *J. Chem. Theory Comput.,* 2013, 9, 1918.
17. (a) T. Lu and F. Chen, *J. Comp. Chem.*, 2012, 33, 580; (b) T. Lu and F. Chen, *J. Mol. Graph. Model.*, 2012, 38, 314.
18. R. F. W. Bader, Atoms in Molecules - A Quantum Theory, *Oxford University Press,* Oxford, 1990.
19. (a) E. R. Johnson, S. Keinan, P. Mori-Sanchez, J. Contreras-Garcia, A J. Cohen and W. Yang, *J. Am. Chem. Soc.* 2010, 132, 6498; (b) J. R. Lane, J. Contreras-García, J. P. Piquemal, B. J. Miller and Henrik G. Kjaergaard, J. Chem. *Theory Comput.*, 2013, 9, 3263; (c) J. Contreras-Garcia, E. Johnson, S. Keinan, R. Chaudret, J.-P. Piquemal, D. Beratan and W. Yang, *J. Chem. Theor. Comp.*, 2011, 7, 625.
20. (a) Gaussian 09, Revision A.02, M. J. Frisch, G. W. Trucks, H. B. Schlegel, G. E. Scuseria, M. A. Robb, J. R. Cheeseman, G. Scalmani, V. Barone, B. Mennucci, G. A. Petersson, H. Nakatsuji, M. Caricato, X. Li, H. P. Hratchian, A. F. Izmaylov, J. Bloino, G. Zheng, J. L. Sonnenberg, M. Hada, M. Ehara, K. Toyota, R. Fukuda, J. Hasegawa, M. Ishida, T. Nakajima, Y. Honda, O. Kitao, H. Nakai, T. Vreven, J. A. Montgomery, Jr., J. E. Peralta, F. Ogliaro, M. Bearpark, J. J. Heyd, E. Brothers, K. N. Kudin, V. N. Staroverov, R. Kobayashi, J. Normand, K. Raghavachari, A. Rendell, J. C. Burant, S. S. Iyengar, J. Tomasi, M. Cossi, N. Rega, J. M. Millam, M. Klene, J. E. Knox, J. B. Cross, V. Bakken, C. Adamo, J. Jaramillo, R. Gomperts, R. E. Stratmann, O. Yazyev, A. J. Austin, R. Cammi, C. Pomelli, J. W. Ochterski, R. L. Martin, K. Morokuma, V. G. Zakrzewski, G. A. Voth, P. Salvador, J. J.

Dannenberg, S. Dapprich, A. D. Daniels, Ö. Farkas, J. B. Foresman, J. V. Ortiz, J. Cioslowski, and D. J. Fox, Gaussian, Inc., Wallingford CT, 2009; (b) M.W.Schmidt, K.K.Baldridge, J.A.Boatz, S.T.Elbert, M.S.Gordon, J.H.Jensen, S.Koseki, N.Matsunaga, K.A.Nguyen, S.Su, T.L.Windus, M.Dupuis and J.A.Montgomery *J. Comput. Chem.*, 1993, 14, 1347.

21. T. A. Keith, AIMAll (Version 11.03.14), 2011. Available via DIALOG at: http://im.tkgristmill.com.
22. W. Humphrey, A. Dalke and K. Schulten, "VMD - Visual Molecular Dynamics", *J. Molec. Graphics*, 1996, 14, 33.
23. (a) P. R. Varadwaj, A. Varadwaj and G. H. Peslherbe, *J. Comput. Chem.*, 2012, 33, 2073; (b) P. R. Varadwaj, *J. Mol. Model.* 16, 2010, 965; (c) P. R. Varadwaj and H. M. Marques, *Phys. Chem. Chem. Phys.,* 2010, 12, 2126; (d) A. Varadwaj and P. R. Varadwaj, *Chem. –Eur. J.*, 2012, 18, 15345.
24. (a) T. Janowski and P. Pulay, *Chem. Phys. Lett.*, 2007, 447, 27; (b) A. Puzder, M. Dion and D. C. Langreth, *J. Chem. Phys.*, 2006, 124, 164105; (c) W. L. Jorgensen and D. L. Severance, *J. Am. Chem. Soc.*, 1990, 11 2, 4168; (d) E. Miliordos, E. Apra and S. S. Xantheas, *J. Phys. Chem. A*, 2014, 118, 7568; (e) Y. C.Park and J. S. Lee, *J. Phys. Chem. A*, 2006, 110, 5091.
25. (a) S. Kumar and A. Das, *J. Chem. Phys.*, 2013, 139, 104311; (b) K. Pluhackova, P. Jurecka and P. Hobza, *Phys. Chem. Chem. Phys.*, 2007, 9, 755; (c) S. Tsuzuki, T. Uchimaru and M. Mikami, *J. Phys. Chem. A*, 2006, 110, 2027-2033.
26. M. R. Battaglia, A. D. Buckingham and J. H. Williams, *Chem. Phys. Lett.*, 1981, 78, 421.
27. (a) C. M. Reddy, M. T. Kirchner, R. C. Gundakaram, K. A. Padmanabhan and G. R. Desiraju, *Chem. –Eur. J.*, 2006, 12, 2222; (b) D. J. R. Duarte, N. M. Peruchena and I. Alkorta, *J. Phys. Chem. A*, 2015, 119, 3746; (c) L. Brammer, G. M. Espallargas and S. Libri, *Cryst. Eng. Comm.*, 2008, 10, 1712; (d) F. F. Awwadi, R. D. Willett, K. A. Peterson and B. Twamley, *Chem. –Eur. J.*, 2006, 12, 8952; (e) D. Chopra, *Cryst. Growth. Des.* 2012, 12, 541.
28. (a) J. P. Perdew and Y. Wang, *Phys. Rev. B*, 1992, 45, 13244; (b) A. D. Becke, *J. Chem. Phys.*, 1993, 98, 1372.
29. P. Su and H. Li, *J. Chem. Phys.*, 2009, 131, 014102.
30. S. Alvarez, *Dalton Trans.*, 2013, 42, 8617.
31. (a) C. F. Matta, N. Castillo and R. J. Boyd, *J. Phys. Chem. A*, 2005, 109, 3669; (b) E. Aubert, S. Lebègue, M. Marsman, T. T. T. Bui, C. Jelsch,. S. Dahaoui,. E. Espinosa and J. G. Angyán, *J. Phys. Chem. A*, 2011, 115, 14484; (c) S. Jenkins, A. Restrepo, J. David, D. Yina and S. R. Kirk, *Phys. Chem. Chem. Phys.*, 2011, 13, 11644; (d) R. F. W. Bader, *J. Phys. Chem. A*, 2009, 113, 10391; (e) I. Alkorta and J. Elguero, *Struct. Chem.*, 2004, 15, 117; (f) C. F. Matta, J. Hernandez-Trujillo, T.-H. Tang and R. F. W. Bader, *Chem. –Eur. J.*, 2003, 9, 1940; (g) T.-H. Tang, E. Deretey, S. J. K. Jensen and I. G. Csizmadia, *Eur. Phys. J. D*, 2006, 37, 217; (h) R. F. W. Bader and C. F. Matta, *Inorg. Chem.*, 2001, 40, 5603; (i) J. Hernández-Trujillo and C. F. Matta, *Struct. Chem.*, 2007, 18, 849; (j) I. Love, *J. Phys. Chem. A*, 2009, 113, 2643.
32. (a) A. M. Pendás, E. Francisco, M. A. Blanco and C. Gatti, *Chem. -Eur. J.*, 2007, 13, 9362; (b) V. Tognetti and L. Joubert, *J. Chem. Phys.*, 2013, 138, 024102; (c) M. A. Blanco, A. M. Pendás and E. Francisco, *J. Chem. Theory Comput.*, 2005, 1, 1096; (d) E. Francisco, A. M. Pendás and M. A. Blanco*, J. Chem. Theory Comput.*, 2006, 2, 90.
33. (a) G. Saleh, C. Gatti, L. L. Presti and J. Contreras-Garcia, *Chem. –Eur. J.*, 2012, 18, 15523; (b) I. Cukrowski, J. H. de Lange and M. Mitoraj, *J. Phys. Chem. A*, 2014, 118, 623; (c) I. González-Veloso, J. A. Carrazana-García, D. Josa, J. Rodríguez-Otero and E. M. Cabaleiro-Lago, *Comput. Theor. Chem.*, 2013, 1053, 123; (d) M. Alonso, T. Woller, F. J. Martin-Martinez, J. Contreras-Garcia, P. Geerlings and F. De Proft, *Chem. –Eur. J.*, 2014, 20, 4845; (e) R. A. Cormanich, R. Rittner, D. O'Hagan and M. Bühl, *J. Phys. Chem. A*, 2014, 118, 7901; (f) E. V. Bartashevich, A. M. Pendás and V. G. Tsirelson, *Phys. Chem. Chem. Phys.*, 2014, 16, 16780.
34. (a) A. Zupan, J. P. Perdew, K. Burke and M. Causá, *Int. J. Qunatum Chem.*, 1997, 61, 865; (b) A. Zupan, K. Burke, E. Ernzerhof and J. P. Perdew, *J. Chem. Phys.*, 1997, 106, 10184.
35. (a) K. Collard and G. G. Hall, *Int. J. Quantum Chem.*, 1977, 12, 623; (b) *C. F. Matta*, R. J. Boyd (Eds.), "The Quantum Theory of Atoms in Molecules: From Solid State to DNA and Drug Design", Wiley-VCH, Weinheim, 2010; (c) S. Jenkins, *Int. J. Quantum Chem.*, 2013, 113, 1603.
36. (a) J. Poater, M. Solá, M. Duran and X. Fradera, *Theor. Chem. Acc.*, 2002, 107, 362; (b) X. Fradera and M. Solá, *J. Comput. Chem.*, 2002, 23, 1347; (c) C. F. Matta, J. Hernandez-Trujillo and R. F. W. Bader, *J. Phys. Chem. A*, 2002, 106, 7369; (d) C. F. Matta and J. Hernandez-Trujillo, J. Phys. Chem. A, 2003, 107, 7496; (f) P. R. Varadwaj, A. Varadwaj, G. H. Peslherbe and H. M. Marques, *J. Phys. Chem. A*, 2011, 115, 13180.
37. (a) H. Sun, K. Ye, C. Wang, H. Qi, F. Li and Y. Wang, J. Phys. Chem. A, 2006, 110, 10750; (b) M. O. Sinnokrot, E. F. Valeev and D. C. Sherrill, *J. Am. Chem. Soc.*, 2002, 124, 10887; (c) M. O. Sinnokrot and D. C. Sherrill, *J. Phys. Chem. A.*, 2004, 108, 10200; (d) S. E. Wheeler and K. N. Houk, *J. Am. Chem. Soc.*, 2008, 130, 10854; (e) S. E. Wheeler and K. N. Houk, *Mol. Phys.*, 2009, 107, 749; (f) S. E. Wheeler and K. N. Houk, *J. Chem. Theory Comput.*, 2009, 5, 2301; (g) T. Smith, L. V. Slipchenko and M. S. Gordon, *J. Phys. Chem. A*, 2008, 112, 5286; (h) E. V. Anslyn and D. A. Dougherty, Modern Physical Organic Chemistry, 1st Edn., University Science Books, Sausalito, California, 2006.

38. (a) M. P. Johansson and M. Swart, *Phys. Chem. Chem. Phys.*, 2013, 15, 11543; (b) P. R. Varadwaj, A. Varadwaj, B.–Y. Jin (manuscript submitted).
39. The Cambridge Structural Database: A quarter of a million crystal structures and rising, F. H. Allen, *Acta Cryst. B* 2002, 58, 380. CSD version 5.36 updates (Nov 2014).
40. R. M. Osuna, V. Hernández, J. T. L. Navarrete, E. Dria and J. J. Novoa, *Theor. Chem. Acc.*, 2011, 128, 541.
41. L. Goerigk, H. Kruse and S. Grimme, *Chem. Phys. Chem.*, 2011, 12, 3412.
42. (a) T. Iikura, T. Tsuneda, T. Yanai and K. Hirao, *J. Chem. Phys.*, 2001, 115, 3540; (b) T. Yanai, D. Tew and N. Handy, *Chem. Phys. Lett.*, 2004, 393, 51.
43. (a) S. F. Boys and F. Bernardai, *Mol. Phys.*, 1970, 553; (b) C. D. Sherrill, Counterpoise Correction and Basis Set Superposition Error, Created on July 21, 2010. Available at: http://vergil.chemistry.gatech.edu/notes/cp.pdf; (c) P. Salvador, B. Paizs, M. Duran and S. Suhai, *J. Comput. Chem.,* 2001, 22, 765.
44. V. Tognetti and L. Joubert, *Phys. Chem. Chem. Phys.*, 2014, 16, 14539.
45. The Gaussian 09 User's Reference, available via: http://www.gaussian.com/g_tech/g_ur/k_dft.htm. Last access August 18, 2015.
46. Y.-K. Han, K. H. Kim, S.-K. Son and Y. S. Lee, *Bull. Korean Chem. Soc.*, 2002, 23, 1271.
47. C. S. Wannere, K. W. Sattelmeyer, H. F. Schaefer III and P. von R. Schleyer, *Angew. Chem.*, 2004, 116, 4296.
48. (a) D. N. Bol'shutkin, V. M. Gasan, A. I. Prokhvatilov and A. I. Erenburg, *Acta Crystallogr., Sect.B : Struct. Crystallogr. Cryst. Chem.*, 1972, 28, 3542; (b) A. N. Fitch, J. K. Cockcroft and Z.Kristallogr, 1993, 203, 29; (c) G. Pepe and J. -M. Gay, *J. Chem. Phys.*, 1989, 90, 5735.
49. (a) P. Jurečka, J. Černý, P. Hobza and D. R. Salahub, *J. Comput. Chem.*, 2007, 28, 555; (b) D. Hugas, S. Simon, and M. Duran, *Chem. Phys. Lett.*, 2004, 386, 373; (c) S. A. C. McDowell, *Chem. Phys. Lett.*, 2006, 424, 239; (d) S. A. C. McDowell, *Chem. Phys. Lett.*, 2014, 598, 1.
50. (a) S. Tsuzuki, K. Honda, T. Uchimaru, M. Mikami, K. Tanabe, *J. Am. Chem. Soc.* 2002, 124, 104; (b) S. Tsuzuki, Interaction with Aromatic Rings, in: Intermolecular Forces and Clusters I (Structure and Bonding), D. Wales, Ed., Springer-Verlag Berlin Heidelberg, *Struc. Bond.,* 2005, 115, 149; (c) P. Hobza, H. L. Selzle, E. W. Schlag, *J. Phys. Chem.* 1996, 100, 18790.
51. (a) R. F. W. Bader, M. E. Stephens, *J. Am. Chem. Soc.,* 1975, 97, 7391; (b) X. Fradera, M. A. Austen, R. F. W. Bader, *J. Phys. Chem. A*, 1999, 103, 304.